JCI The Journal of Clinical Investigation

West Nile virus triggers intestinal dysmotility via T cell-mediated enteric nervous system injury

Hana Janova, … , Thaddeus S. Stappenbeck, Michael S. Diamond

J Clin Invest. 2024. https://doi.org/10.1172/JCI181421.

Research In-Press Preview Gastroenterology Infectious disease

Graphical abstract

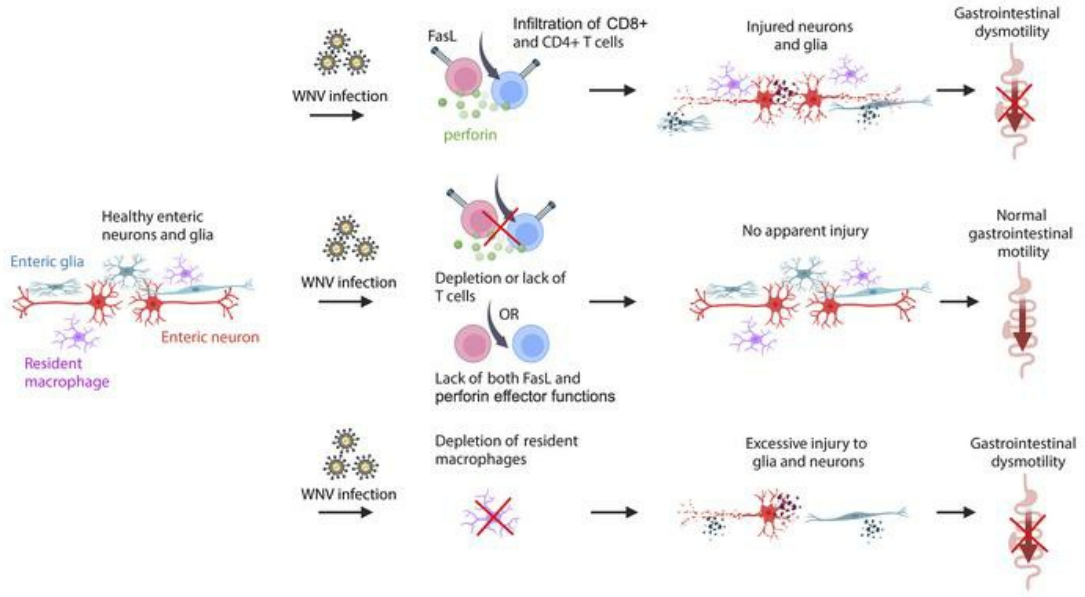

West Nile virus triggers intestinal dysmotility via T cell-mediated enteric nervous system injury

Hana Janova[1], Fang R. Zhao[1], Pritesh Desai[1], Matthias Mack[2], Larissa B. Thackray[1], Thaddeus S. Stappenbeck[3]*, and Michael S. Diamond[1,4,5,6]*

[1]Department of Medicine, Washington University School of Medicine, Saint Louis, MO 63110, USA

[2]Department of Nephrology, University Hospital Regensburg, Regensburg, Germany

[3]Department of Inflammation and Immunity, Cleveland Clinic, Cleveland, OH 44195

[4]Department of Pathology and Immunology, Washington University School of Medicine, Saint Louis, MO 63110

[5]Department of Molecular Microbiology, Washington University School of Medicine, Saint Louis, MO 63110

[6]The Andrew M. and Jane M. Bursky Center for Human Immunology and Immunotherapy Programs, Washington University School of Medicine, Saint Louis, MO 63110

*Corresponding authors:

Thaddeus S, Stappenbeck, stappet@ccf.org; 216-444-3082; Department of Inflammation and Immunity; Lerner Research Institute, Cleveland Clinic, Cleveland, OH 44195

Michael S. Diamond, M.D., Ph.D., mdiamond@wustl.edu; 314-362-2842; Department of Medicine, Washington University School of Medicine, Box 8051; Saint Louis, MO 63110

Conflict of interest: M.S.D. is a consultant or advisor for Inbios, VIR Biotechnology, Moderna, Merck, GlaxoSmithKline, IntegerBio, and Akagera Medicines. The Diamond laboratory has

26 received unrelated funding support in sponsored research agreements from Moderna, VIR
27 Biotechnology, IntegerBio and Emergent BioSolutions.

ABSTRACT

Intestinal dysmotility syndromes have been epidemiologically associated with several antecedent bacterial and viral infections. To model this phenotype, we previously infected mice with the neurotropic flavivirus, West Nile Virus (WNV) and demonstrated intestinal transit defects. Here, we find that within one week of WNV infection, enteric neurons and glia become damaged, resulting in sustained reductions of neuronal cells and their networks of connecting fibers. Using cell-depleting antibodies, adoptive transfer experiments, and mice lacking specific immune cells or immune functions, we show that infiltrating WNV-specific $CD4^+$ and $CD8^+$ T cells damage the enteric nervous system (ENS) and glia, which leads to intestinal dysmotility; these T cells use multiple and redundant effector functions including perforin and Fas ligand. In comparison, WNV-triggered ENS injury and intestinal dysmotility appears to not require infiltrating monocytes and damage may be limited by resident muscularis macrophages. Overall, our experiments support a model whereby antigen specific T cell subsets and their effector molecules responding to WNV infection direct immune pathology against enteric neurons and supporting glia that results in intestinal dysmotility.

INTRODUCTION

Properly regulated intestinal motility allows for efficient timing of nutrient uptake and elimination of waste. Peristalsis of the intestines is regulated primarily by the peripheral enteric nervous system (ENS) with neural inputs from the central nervous system (CNS) (1). The neuronal bodies of the ENS are concentrated in ganglia and embedded in two interconnected plexi: the submucosal plexus in the submucosa, and the myenteric plexus, positioned between the inner circular and outer longitudinal smooth muscle layers of the intestine. Enteric neurons function with other cells including glia, interstitial cells of Cajal (ICCs), and muscularis macrophages to regulate intestinal motility. Injury, dysfunction, or depletion of any of these cells can result in intestinal dysmotility (2-8).

It is estimated that more than 40% of human adults suffer at some point during their lifetime from some form of chronic gastrointestinal (GI) motility disorder, which negatively affects quality of life (9, 10). Although age, sex, genetics, diet, and socioeconomic factors are associated with the development of these disorders, antecedent GI tract infections with bacteria or viruses are thought to have roles in triggering intestinal dysmotility (11). Despite the prevalence of GI tract motility disorders, components of the underlying mechanisms of injury have been established experimentally in only a few instances. In mice, enteric infection with the bacteria *Salmonella typhimurium* triggers long-term GI tract dysmotility due to loss of neurons via caspase-1 and -11-dependent apoptosis (12). Systemic infection of mice with herpes simplex virus (HSV-1) causes acute injury to enteric neurons and glia through a mechanism requiring neutrophils or macrophages that produce reactive oxygen and nitrogen species (13, 14). West Nile virus (WNV), a mosquito-transmitted flavivirus, can infect neurons in the small intestine after subcutaneous inoculation and viremic spread to cause acute and relapsing GI tract dysmotility (2).

Although WNV infection damages the ENS (2), the mechanisms and targets of injury remain poorly understood. Here, we show that WNV infection caused injury to the ENS and glial networks. Although infiltrating monocytes and monocyte-derived macrophages in the myenteric

plexus and the muscular layers of the small intestine were present at multiple time points after WNV infection, genetic depletion or inhibition of their recruitment did not prevent damage to the neuronal network or affect WNV-triggered GI dysmotility. Rather, using multiple transgenic mouse strains and by performing immune cell depletions and adoptive transfer studies, we showed that WNV-specific $CD4^+$ and $CD8^+$ T cells used several different effector mechanisms (including perforin and FasL) to damage enteric neurons and neighboring glial cells leading to GI transit dysfunction. Moreover, this T cell-mediated injury was worsened by the depletion of resident muscularis macrophages. Overall, our study defines how both resident and infiltrating innate and adaptive immune cells in the GI tract respond to viral infection to reshape the ENS architecture with consequences for intestinal motility.

RESULTS

WNV infection triggers persistent changes in the enteric neuronal network. Our previous work described a dysmotility syndrome after WNV infection with preferential effects in the small intestine (2). WNV antigen localizes to enteric neurons of the small intestine during the acute phase of infection (at 6 days post-infection [dpi]) after subcutaneous inoculation (2); however, the viral tropism for specific neuronal populations is unclear. To address this question, we inoculated *ChAT-eGFP* reporter mice, which identify cholinergic neurons, with WNV (Figure 1A) and co-stained whole mount tissue preparations of small intestines with antisera against WNV (15) as well as for other neuronal subsets. WNV antigen was detected in similar percentages of calretinin$^+$, ChAT$^+$, and nNOS$^+$ neurons (Figure 1B-C and Supplemental Figure S1A-C). WNV antigen in the myenteric and submucosal plexuses varied along the length of the small intestine, with the middle (jejunal) and distal (ileal) segments showing the highest penetrance (~70-90% of mice) and the proximal (duodenal) region having less penetrance (20-33% of mice) (Figure 1D and Supplemental Figure S1D). Thus, we focused subsequent analyses on the middle and distal regions of the small intestine.

To assess the impact of WNV infection in the small intestine, we first quantified the number of HuC/D$^+$ neuronal bodies in whole mount tissue preparations. In the myenteric plexus, neuronal cell body numbers were decreased in the middle and distal regions of the small intestine at 7 dpi as compared to mock infected controls (Figure 1E and H). Similarly, we observed lower numbers of HuC/D$^+$ neurons in the submucosal plexus of the middle region of the small intestine (Figure 1E). The loss of neuronal bodies within intestinal ganglia after WNV infection was associated with a decreased density of their axonal fiber networks (herein as neuronal network density) in the myenteric plexus and the inner circular muscle layer of the muscularis propria in the middle and distal regions of the small intestine at 7 dpi; this included a reduction of calretinin$^+$ and nNOS$^+$ networks that are major neuronal subsets in the myenteric plexus and inner circular muscle layer (Figure 1F, H and Supplemental Figure S1E-H). In contrast, the density of serotonergic myenteric

neuronal networks (*i.e.*, those secreting 5-hydroxytryptamine; 5-HT) in the myenteric plexus at 7 dpi was not different from sham-infected controls (Figure 1F and H). In the submucosal plexus, the calretinin$^+$ neuronal network density also was diminished with WNV infection, which corresponded to the decreased numbers of neurons (Figure 1G-H). However, as submucosal plexus neurons do not contribute substantially to GI motility (16), we focused on the neuronal cells and networks in the myenteric plexus.

As the dysmotility after WNV infection can persist through 65 days (Supplemental Figure S1I and (2)), we quantified the number of HuC/D$^+$ neurons and assessed the neuronal network density in the myenteric plexus at later times post infection: 15 dpi (subacute phase), 28 dpi (chronic phase) and 65 dpi (late chronic, convalescent phase) (Figure 1A). By 65 dpi, the numbers of HuC/D$^+$ neurons in the distal small intestine showed near complete recovery, a process that began as early as 15 dpi (Figure 1I). However, this recovery did not occur to the same extent in the middle region of the small intestine, as fewer neurons were detected at 65 dpi than in sham-infected controls. Our analysis of neuronal networks showed a durable loss of the density of nNOS$^+$ and calretinin$^+$ neuronal networks (Figure 1J) at 15, 28, and 65 dpi in both the middle and distal regions of the small intestine. In contrast, differences in neuronal network density were not detected in the proximal region of the small intestine at 28 dpi, a region that has less viral antigen detected at 6 dpi (Supplemental Figure S1C and L). Although skewing of neuronal subgroup proportions can affect GI motility (7, 17), we did not detect differences in proportions of nNOS$^+$ or calretinin$^+$ neurons at any time point after WNV infection (Supplemental Figure S1J-K). However, WNV infection caused a marked loss in density of 5-HT$^+$ neuronal processes at 15, 28, and 65 dpi in the middle and distal small intestine (Figure 1K). This neuronal subset is important for the formation of new neurons after intestinal injury (18, 19).

To identify factors that might regulate the ENS response to WNV infection in the acute phase (6 dpi), we performed a translating ribosomal affinity purification (TRAP) of the muscularis externa of WNV and mock-infected *Snap25l10a* GFP mice. *Snap25l10a* GFP mice express a

GFP-tagged ribosomal subunit 10la in all neurons, which enables isolation of RNA predominantly from neurons (Supplemental Figure S1M). RNA sequencing showed increased expression of antiviral genes and pathways (*e.g.*, IFN-stimulated genes (ISGs), *Ifit* family members, *Stat1/2* pathways, and pattern recognition receptor signaling pathways) (Figure 1L-N and Supplemental Figure S1N). We also observed higher levels of mRNAs encoding *Ccl6*, *Ccl3*, *Cxcl10*, and *Ccl2* cytokines that stimulate chemotaxis of T cells, monocytes, and macrophages (Figure 1O). Furthermore, WNV infection led to an increase in transcripts associated with antigen presentation, including components of MHC class I (*Tap1, B2m*) and MHC class II (*H2-DMb1*) antigen processing (Supplemental Figure S1O and P). These RNAseq data identified gene signatures in a neuron-enriched population from the muscularis externa with possible antiviral, immune cell trafficking, and immunomodulatory effects in response to viral infection.

WNV infection triggers persistent changes in intestinal glial cell networks. Enteric glia provide structural and metabolic support for enteric neurons and contribute to neurogenesis (20-25). To determine whether the glial network is affected by WNV infection, we evaluated intestinal whole mounts from WNV infected mice at 7 dpi by co-immunostaining with antisera against WNV and antibodies to the pan-glial marker S100β (20). Despite limited detection of WNV-antigen$^+$ glial cells (Supplemental Figure S2A), the S100β$^+$ glial network density in the myenteric plexus was markedly diminished in WNV-infected mice at 7 dpi (Figure 2A-B) with sustained reductions also observed at 28 dpi and 65 dpi (Figure 2C). However, not all neuronal associated networks in the ENS showed diminished density following WNV infection. ICCs located in the smooth muscle layer act as transducers of signals from enteric neurons to smooth muscle cells (8). Although WNV antigen localized sporadically to ICCs in the circular muscle layer of the small intestine at 6 dpi (Supplemental Figure S2B), their density, as judged by cKit staining (26) was like that of sham-treated mice at 15, 28, or 65 dpi (Supplemental Figure S2C).

Monocyte and macrophage infiltration are not required for ENS damage and intestinal dysmotility following WNV infection. Monocytes and monocyte-derived

157 macrophages have been shown to injure the intestine in the context of herpesvirus infection (27).
158 Given our data showing higher levels of myeloid cell chemoattractant mRNAs (*e.g.*, *Ccl2*, *Ccl3*,
159 *Ccl6*, and *Ccl9*) in the muscularis externa of WNV-infected mice (Figure 1O), we quantified
160 monocyte accumulation at 6 dpi in the small intestine of WNV-infected mice using heterozygous
161 *Ccr2*-GFP reporter mice after staining whole mount preparations for Iba1, a marker of monocyte-
162 derived macrophages and endogenous muscularis macrophages but not recent monocyte
163 immigrants (28, 29). Both monocytes (*Ccr2*-GFP$^+$ Iba1$^-$ cells) and macrophages (*Ccr2*-GFP$^+$ Iba1$^+$
164 cells) were increased in number in the proximity of WNV-infected neurons at 6 dpi; the elevation
165 of monocytes persisted up to 15 dpi in the myenteric plexus and the circular inner smooth muscle
166 layer of the muscularis externa (Figure 3A-B and C-E). Elevated numbers of macrophages (Iba1$^+$
167 cells) persisted through 65 dpi with a peak at 15 dpi (Figure 3C and F-G). Fate mapping studies
168 using *Ccr2* CreER YFP reporter mice demonstrated that the increased number of macrophages
169 was due to infiltrating monocytes, since most of the Iba1$^+$ cells also expressed YFP (Supplemental
170 Figure S3A).
171 To assess the role of the infiltrating monocytes in delaying GI transit in WNV infected mice,
172 we inhibited their migration into the intestines by using an anti-CCR2 blocking monoclonal
173 antibody (mAb) (30) or *Ccr2*$^{-/-}$ mice (Supplemental Figure S3B-C). We found that reduced
174 accumulation of monocytes during acute WNV infection did not prevent damage to neuronal and
175 glial networks at 7 dpi and did not affect the delayed GI transit time phenotype at 7 or 15 dpi
176 (Figure 3H-I and Supplemental Figure S3D-G). Neutrophil infiltration causes injury to enteric
177 neurons and GI dysmotility after herpesvirus infection in mice (13) and can contribute to WNV-
178 induced pathogenesis in the brain (31-33). However, complete and partial depletion of neutrophils
179 and monocytes, respectively, with an anti-Ly6G/Ly6C mAb (Gr-1) did not improve WNV-induced
180 GI tract dysmotility at 7 dpi (Supplemental Figure S3B and H-J). We confirmed this result by
181 injecting *Ccr2*$^{-/-}$ mice with anti-Ly6G/Ly6C mAb to ensure that a lack of monocyte infiltration during
182 WNV infection was not compensated by an increased influx of neutrophils (34) (Supplemental

Figure S3B and K-L). Thus, WNV-induced intestinal dysmotility appears independent of both infiltrating monocytes and neutrophils.

Resident muscularis macrophages may reduce excessive damage to neuronal and glial networks of WNV-infected mice. Resident macrophages of the GI tract have been proposed to protect the ENS during bacterial infection by preventing neuronal cell death (12). To address their role after WNV infection, we injected mice with anti-CSF1R mAb, which depletes muscularis macrophages, as confirmed by quantification of Iba1$^+$ cells in the myenteric plexus (Supplemental Figure S3M-N). Animals depleted of muscular macrophages did not show improvement in delayed GI transit times at 7 dpi compared to those given an isotype control mAb (Figure 3J). This GI defect was not caused by a compensatory infiltration of monocytes or monocyte-derived macrophages, as WNV-infected *Ccr2*$^{-/-}$ mice treated with anti-CSF1R antibody had similar GI transit delays (Supplemental Figure S3O). However, mice deficient in resident macrophages showed a greater loss of neuronal and glial networks than isotype control mAb treated mice after WNV infection (Figure 3K-M). Thus, resident muscularis macrophages appear to prevent excessive damage to neuronal and glial network during WNV infection.

Damage to neuronal and glial networks is caused by T cells. We previously noted that CD8$^+$ T cells likely contribute to GI tract dysmotility after WNV infection (2). However, these studies were performed with *Cd8α*$^{-/-}$ mice, which lack CD8$^+$ T cells, but retain other T cell subsets (35). Moreover, the effects of WNV infection on the neuronal network in *Cd8α*$^{-/-}$ mice were not evaluated. To measure GI tract motility and analyze the neuronal and glial network in the absence of all T cells, *TCRbd*$^{-/-}$ mice, which lack both αβ and γδ T cells, were inoculated with WNV. Since mice lacking T cells develop uncontrolled CNS infection and succumb within 10 to 14 days (36-40), we only performed analyses at 7 dpi. Notably, WNV-infected *TCRbd*$^{-/-}$ mice did not show GI tract dysmotility or reduced density of nNOS$^+$ and calretinin$^+$ neuronal networks in the myenteric plexus as compared to wild-type (wt) littermate controls; infected *TCRbd*$^{-/-}$ mice appeared similar to sham-infected wt or *TCRbd*$^{-/-}$ mice (Figure 4A-B), despite the high levels of viral antigen in the

myenteric plexus (Figure 4C and Supplemental Figure S4A). Similarly, at 7 dpi, the glial network in the myenteric plexus was unaffected in WNV-infected *TCRbd*$^{-/-}$ mice (Figure 4D). In the absence of T cells, the numbers of HuC/D^{+} neurons in the submucosal plexus also were not affected by WNV infection, although the density of the calretinin^{+} network was decreased (Supplemental Figure S4B). These results are consistent with a role for T cells in mediating the injury of motor neurons and glial cells in the myenteric plexus and development of GI tract dysmotility during the acute phase of WNV infection. However, submucosal neurons may be injured by T cell-independent mechanisms. Because *TCRbd*$^{-/-}$ mice also have some defects in B cell development and differentiation (41), we performed additional experiments in μMT mice that lack mature B cells and antibody. As WNV-infected μMT and wt littermate mice showed similarly delayed GI transit times at 7 dpi (Supplemental Figure S4C), mature B cells or antibody are not required for WNV-triggered GI dysmotility.

We next evaluated the specific roles of CD4^{+} and CD8^{+} T cells in WNV-triggered intestinal dysmotility. Flow cytometric analysis and whole mount staining showed that during the acute phase of WNV infection (days 6 and 7), CD4^{+} and CD8^{+} T cells accumulated in the areas of the muscularis externa adjacent to damaged neurons (Figure 4E and Supplemental Figure S4D-E). To assess the individual contributions of CD4^{+} and CD8^{+} T cells to WNV-induced GI dysmotility, we treated mice with depleting mAbs that target these T cell subsets (Supplemental Figure S4F). We chose this approach because *Cd4*$^{-/-}$ mice also have altered CD8^{+} T cell development due to lineage commitment effects during thymopoiesis (42). Mice treated with anti-CD4 or anti-CD8β antibodies all demonstrated targeted cell depletion in the muscularis externa of the small intestine, the spleen, and Peyer's patches (Supplemental Figure S4G-I). While treatment with either anti-CD4 or anti-CD8β mAbs alone did not rescue intestinal motility at 7 dpi, administration of both anti-CD4 and anti-CD8β mAbs restored intestinal motility to homeostatic levels in most animals (Figure 4F), and this was associated with improved neuronal and glial networks in the myenteric

plexus after WNV infection (Figure 4G-H). These results are similar to those observed in WNV-infected *TCRbd*$^{-/-}$ mice, supporting a role for both CD4$^+$ and CD8$^+$ T cells in the damage of neuronal and glial network and the intestinal dysmotility after WNV infection.

Antigen-specific CD4$^+$ and CD8$^+$ T cells cause neuronal and glial injury after WNV infection. To further dissect the specific contribution of CD4$^+$ and CD8$^+$ T cells in WNV-infected mice to causing neuronal and glial damage, we isolated WNV-primed CD4$^+$ and CD8$^+$ T cells from wt mice at 7 dpi and adoptively transferred them into WNV-infected *TCRbd*$^{-/-}$ mice at 2 dpi (Supplemental Figure S5A). Subsequently, we analyzed intestinal tract motility and injury to neurons and glia at 7 dpi (Figure 5A-E) after confirming the efficiency of the T cell transfers (Supplemental Figure S5B-C). More than 50% of *TCRbd*$^{-/-}$ mice receiving CD8$^+$ T cells developed severe GI tract dysmotility (≥ 360 min) and showed damage to neuronal and glial networks, whereas sham or WNV-infected *TCRbd*$^{-/-}$ mice without T cell transfers did not (Figure 5A-E). While most WNV-infected mice injected with CD4$^+$ T cells did not show delayed GI tract transit times, we still observed injury to neurons (Figure 5A-E). Together, these results suggest that while both CD4$^+$ and CD8$^+$ T cells can injure the neuronal network, CD8$^+$ T cells trigger greater damage resulting in intestinal dysmotility.

Virus-specific and bystander effector CD8$^+$ T cells can target infected cells for lysis and promote local inflammation (43). To determine the role of antigen-specific recognition of target cells by CD8$^+$ T cells in ENS injury, we stained cells with D^b-restricted tetramers that recognize an immunodominant peptide epitope (SSVWNATTAI) in the WNV NS4B protein(44). In WNV-infected small intestines, approximately 25% of CD8$^+$ T cells in the muscularis externa (and 10% in the remainder of the small intestine) were specific for the NS4B immunodominant peptide (Figure 5F). To determine the contributions of antigen-specific and bystander CD8$^+$ T cells in causing damage to neurons and glia after WNV infection, we utilized T cell receptor (TCR) transgenic mice in which the vast majority of CD8$^+$ T cells are specific for the WNV NS4B peptide

epitope or, as a control, for the lymphocytic choriomeningitis virus (LCMV) gp33 peptide epitope (KAVYNFATC) (45-47). Transgenic WNV NS4B or LCMV gp33 $CD8^+$ T cells were adoptively transferred into *TCRbd*$^{-/-}$ mice and, one day later, recipient animals were inoculated subcutaneously with WNV (Supplemental Figure S5D-E). At 7 dpi, we measured intestinal tract motility, collected mesenteric lymph nodes to confirm T cell colonization (Supplemental Figure S5F), and analyzed the neuronal and glial networks from the middle and distal regions of the small intestine. Whereas *TCRbd*$^{-/-}$ mice given NS4B-specific $CD8^+$ T cells showed delayed intestinal transit times and damage to neuronal and glial networks in the middle and distal regions of the small intestine, animals given LCMV gp33-specific (P14) $CD8^+$ T cells did not develop dysmotility (Figure 5G-I). Nonetheless, WNV-infected *TCRbd*$^{-/-}$ mice that received LCMV-specific $CD8^+$ T cells showed some damage to neuronal networks (Figure 5H), suggesting either limited bystander injury mediated by antigen non-specific $CD8^+$ T cells or expansion of WNV-specific $CD8^+$ T cells from the small repertoire of endogenous TCRs in LCMV gp33 (P14) TCR transgenic mice in a wt C57BL/6 background.

To further assess a potential role of bystander $CD8^+$ T cells, we crossed the LCMV P14 transgenic mice with *Rag1*$^{-/-}$ mice to generate animals in which virtually every $CD8^+$ T cell is specific for the LCMV gp33 peptide (Supplemental Figure S5G); these animals also lack $CD4^+$ T cells. We measured the intestinal transit in wt and *P14 Rag1*$^{-/-}$ mice at 7 days before (baseline) and after WNV infection (Supplemental Figure S5G-I). Notably, WNV-infected *P14 Rag1*$^{-/-}$ mice showed normal GI tract transit at day 7, comparable to baseline or sham-infected wt mice (Supplemental Figure S5H). Similarly, we did not observe damage to neuronal and glial network in WNV-infected *P14 Rag1*$^{-/-}$ mice (Supplemental Figure S5I). Collectively, these results do not support a substantive role for bystander $CD8^+$ T cells in neuronal and glial injury in the context of WNV infection.

We similarly assessed the role of bystander $CD4^+$ T cells on ENS integrity and function after WNV infection, by crossing OT-II TCR transgenic mice with *Rag1*$^{-/-}$ mice to generate mice

285 that lack $CD8^+$ T cells and have $CD4^+$ T cells that are specific for the ovalbumin peptide 323-339
286 (OVA; ISQAVHAAHAEINEAGR) (Supplemental Figure S5J). At 7 dpi, none of the WNV-infected
287 *OTII Rag1*$^{-/-}$ mice exhibited intestinal dysmotility, and neuronal networks appeared normal
288 (Supplemental Figure S5K-L). Thus, bystander $CD4^+$ T cells also do not induce neuronal injury
289 and GI dysmotility after WNV infection.

290 **$CD4^+$ and $CD8^+$ T cells cause neuron and glia injury using multiple effector**
291 **mechanisms.** T cells can use a variety of mechanisms to clear WNV-infected neurons from the
292 brain including cytotoxic granules (perforin/granzymes), pro-inflammatory cytokines (*e.g.*, TNF
293 and IFNγ), and death receptor signaling pathways (Fas ligand (FasL) or TRAIL) (37, 48-52). To
294 determine the contribution of these T cell effector mechanisms to ENS damage after WNV
295 infection, we used a combination of genetic and pharmacological loss-of-function approaches to
296 test the role of perforin (*Prf1*$^{-/-}$ mice), FasL (*gld* mutant; *Fasl*$^{gld/gld}$ mice), IFNγ (*Ifngr*$^{-/-}$ mice), and
297 TNF (blocking mAb, MP6-XT22 that inhibits both membrane-associated and soluble forms (53)).
298 At 7 dpi, WNV-infected *Prf1*$^{-/-}$, *Fasl*$^{gld/gld}$, and *Ifngr*$^{-/-}$ mice all showed delayed GI transit like wt
299 littermate controls (Figure 6A-C). Wt mice treated with an anti-TNF mAb (MP6-XT22) also showed
300 delayed GI transit times after WNV infection similar to controls (Figure 6D and Supplemental
301 Figure S6A). In addition, we observed similar or even greater intestinal segment dilation in WNV-
302 infected *Prf1*$^{-/-}$, *Fasl*$^{gld/gld}$, or *Ifngr*$^{-/-}$ mice or anti-TNF-treated mice compared to WNV-infected
303 controls (Supplemental Figure S6B). Although we observed damage to the neuronal networks
304 and high numbers of $CD3^+$ T cells in the myenteric plexus in WNV-infected *Prf1*$^{-/-}$ and *Fasl*$^{gld/gld}$
305 mice, the glial network appeared more intact in these two strains (Figure 6E-F and Supplemental
306 Figure S6C-D). These data suggest that loss of individual cytolytic pathways or effector cytokines
307 was not sufficient to ameliorate the WNV-induced damage of neurons and intestinal dysmotility,
308 although glia can be affected.

309 Activated $CD4^+$ and $CD8^+$ T cells can both have cytolytic activity (54) and produce
310 inflammatory cytokines after WNV antigen stimulation (37, 55). Flow cytometric analysis revealed

that perforin was present in almost all $CD8^+$ T cells and on average, 25% of $CD4^+$ T cells in the muscularis layer of WNV-infected mice at 7 dpi (Figure 6G). As multiple effector functions in different T cell populations could be used concurrently to target WNV-infected cells, we hypothesized possible redundancy in effector mechanisms that cause injury to enteric neurons. To test this hypothesis, prior to WNV infection, we depleted $CD4^+$ or $CD8^+$ T cells in either *Prf1*$^{-/-}$, *Fasl*$^{gld/gld}$, *or Ifngr*$^{-/-}$ mice or in wt mice treated with blocking mAbs against IFNγ (Supplemental Figure S6A). Depletion of $CD4^+$ or $CD8^+$ T cells did not mitigate GI transit defects in either WNV-infected *Ifngr*$^{-/-}$ mice or wt mice treated with IFNγ blocking mAb (Supplemental Figure S6E-F). However, depletion of $CD8^+$, but not $CD4^+$, T cells in *Prf1*$^{-/-}$ or *Fasl*$^{gld/gld}$ mice normalized the GI transit time defect and prevented damage to neuronal networks (Figure 6H-L and Supplemental Figure S6G). These data suggest that (i) $CD8^+$ T cells can utilize an alternative cytolytic mechanism in the absence of perforin and (ii) $CD4^+$ T cells require both perforin and FasL pathways to mediate WNV-induced damage and dysmotility in the context of a $CD8^+$ T cell deficiency. Thus, T cells can use multiple effector mechanisms to target WNV-infected neuronal cells in the small intestine.

Mice lacking both perforin and FasL do not develop gastrointestinal dysmotility and have intact neuronal and glial networks. FasL and perforin can function together to augment cytotoxic T cell responses (56). To more definitively determine whether perforin and FasL together are the dominant mechanisms causing neuronal and glial injury and ensuing GI dysmotility after WNV infection, we generated double-knock out (*DKO*) mice by crossing *Prf1*$^{-/-}$ and *Fasl*$^{gld/gld}$ mice (Figure 7A). We inoculated DKO (*Prf1*$^{-/-}$*; Fasl*$^{gld/gld}$) subcutaneously with WNV and at 7 dpi measured the GI transit time and analyzed neuronal and glial networks in the small intestine. Most WNV-infected DKO mice showed normal GI motility and an absence of bowel dilation (Figure 7B-C). Consistent with these results, the neuronal and glial networks were intact in WNV-infected DKO mice and like those of uninfected wt mice (Figure 7D-E), despite the presence of WNV antigen and $CD3^+$ T cells in the myenteric plexus of DKO mice (Figure 7F-G). These results

337 indicate that in mice containing both $CD4^+$ and $CD8^+$ T cells, either FasL or perforin is sufficient
338 to cause the WNV-triggered pathology in the gut. When both effector mechanisms or T cells were
339 absent, WNV-induced defects in GI motility and neuronal and glial network injury were prevented.

DISCUSSION

In this study, we show that WNV infection damages enteric neuronal and glial networks, and this injury is associated with reduced intestinal motility. Acute WNV infection causes loss of neuronal bodies in both the myenteric and submucosal plexuses and diminished density of neuronal fibers in the circular muscle layer. We observe a durable loss of neurons in the middle region of small intestine, which is associated with a lower density in the networks of major neuronal subgroups (calretinin$^+$ and nNOS$^+$) and 5-HT$^+$ interneurons. These neuronal defects may be perpetuated by the presence of persistent WNV RNA in the intestine (2). Persistent viral RNA can be detected directly or indirectly by immune cells, which can produce pro-inflammatory mediators or recruit cells that contribute to the continued loss of neuronal networks and hinder recovery. Despite an accumulation of monocytes and macrophages at the site of neuronal infection in the proximity of the myenteric plexus, infection-induced injury to neurons and glia is caused principally by WNV-specific CD8$^+$ T cells with a contribution from CD4$^+$ T cells. Furthermore, the T cell-mediated injury of ENS components is mediated by a combination of multiple redundant effector functions, including Fas-FasL signaling and perforin, that contribute to the damage of neurons and glia. When both effector mechanisms are absent, the intestinal dysmotility and damage to neuronal and glial networks following WNV infection are prevented.

The damage to the enteric glia by WNV is important, as these cells express receptors for neurotransmitters that sustain neuronal circuits and regulate GI motility (4, 20, 57, 58). To date, no studies have shown the extent of enteric glia damage during viral or bacterial infection. Despite being infected by WNV at lower frequency than neurons, glial networks and processes were diminished during the acute phase of WNV infection. Although direct infection could have a role in glial injury, the inflammatory environment or actions of infiltrating immune cells also may contribute to their damage. A loss of S100β$^+$ glia cells or glial networks was linked previously to increased proinflammatory cytokine levels (*e.g.*, IFNγ and TNFα) in patients with inflammatory bowel disease (59). Our data suggest that T cells use cytolytic mechanisms (perforin or Fas-FasL

366 signaling) to induce glial injury in the context of WNV infection. The damage to both neurons and
367 glia during the acute phase of infection likely exacerbates the GI dysmotility phenotype. The
368 persistent reduction of the glial network, especially in the middle (jejunal) region of small intestine,
369 also likely adversely impacts recovery of the ENS, as glia can serve as a source of new neurons
370 via differentiation after injury and produce glia cell-derived neurotrophic factor (GDNF) and nerve
371 growth factor (NGF) (24, 60-62).

372 The dysmotility associated with relative loss of specific neuronal subpopulations was reported
373 in response to other types of viral and bacterial intestinal infection (7), although in contrast to
374 these studies, we did not observe differences in the ratios of the major nNOS$^+$ and calretinin$^+$
375 subpopulations after WNV infection. Instead, WNV triggered losses in the axonal network of
376 serotonergic neurons. While we did not observe a decrease in the axonal network of serotonergic
377 neurons during the acute phase of WNV infection, we detected durable losses of the serotonergic
378 neurons in the myenteric plexus at 14 dpi and through 65 dpi. Although their precise role in GI
379 motility has been debated (63), the disruption of serotonergic neuronal signaling after WNV
380 infection might delay the replenishment and repair of neuronal networks through effects on
381 neurogenesis (18).

382 In the context of tissue inflammation, infiltrating monocytes can differentiate into
383 macrophages and produce pro-inflammatory mediators including TNF, IL-6, IL-1β, and reactive
384 oxygen species. After HSV-1 infection or in an experimental model of inflammatory bowel disease,
385 Ly6C^{hi} CCR2$^+$ monocytes and derived macrophages contributed to the damage to enteric neurons
386 (27, 64, 65). Although CCR2$^+$ monocytes and newly differentiated macrophages (Iba1$^+$ CCR2$^+$)
387 localize near WNV-infected neurons at 6 dpi and persist through 15 dpi, acquired or genetic
388 depletion of monocytes did not prevent the neuronal damage and the ensuing WNV-induced GI
389 tract dysmotility. Thus, WNV-triggered dysmotility during the acute phase appears to be
390 independent of the actions of infiltrating monocytes and monocyte-derived macrophages.
391 Moreover, resident muscularis macrophages also did not contribute to the ENS damage. Instead,

depletion studies showed that resident muscularis macrophages limited neuronal death and glial injury in WNV-infected intestines, which supports findings showing their protective effects in the context of some bacterial infections (12, 66). Although the mechanistic link to protection by muscularis macrophages remains unclear, we noted higher levels of *Ccl6* in our neuron-enriched RNAseq analysis, which is thought to polarize macrophages towards a “pro-healing” phenotype (67).

Our prior study suggested that T cells in the GI tract contribute to motility defects after WNV infection (2). We extended these results using antibody depletions, genetically deficient mice, and adoptive transfer experiments, which together established contributory and pathogenic roles for both $CD4^+$ and $CD8^+$ T cells. We show that *TCRbd*$^{-/-}$ mice lacking both $CD4^+$ and $CD8^+$ T cells have intact neuronal networks in the myenteric but not the submucosal plexus. This discrepancy might be due to the position of the submucosal neurons closer to the lamina propria, where other innate immune cells are located and could contribute to neuronal damage. Transfer of $CD8^+$ T cells from WNV-primed wt mice or naïve WNV NS4B peptide TCR transgenic mice into recipient *TCRbd*$^{-/-}$ mice resulted in dysmotility and injury to the neuronal networks in the context of WNV infection. However, experiments with OT-II or P14 LCMV transgenic mice suggested that the damage was principally mediated by antigen-specific and not bystander T cells. Even though bystander T cells can mediate protective or pathogenic roles in the context of some viral infections (68, 69), we did not observe substantive contributions by these cells to ENS injury.

Whereas adoptive transfer of WNV-primed wt $CD8^+$ T cells to WNV-infected *TCRbd*$^{-/-}$ mice was sufficient to induce GI dysmotility in more than 60% of mice, few mice showed severe ENS damage, and the glial network density was not significantly decreased. Moreover, adoptive transfer of $CD4^+$ T cells from WNV-infected wt mice to WNV-infected *TCRbd*$^{-/-}$ mice triggered low levels of neuronal damage, which was not sufficient to cause severe GI dysmotility. These partial phenotypes are consistent with our observation that in wt mice, depletion of both $CD4^+$ and $CD8^+$ T cell populations was required to prevent GI tract injury and dysmotility after WNV infection.

While WNV-specific $CD8^+$ T cells appear to be the dominant mediators of neuronal damage and intestinal transit dysfunction, there are clearly contributory pathological effects of $CD4^+$ T cells, which are capable of inducing dysmotility in WNV-infected mice when $CD8^+$ T cells are depleted. Redundant pathogenic roles of $CD4^+$ and $CD8^+$ T cells were described for mouse hepatitis virus (MHV) in the context of demyelination in the brain (70, 71). During MHV infection, IFNγ produced by $CD8^+$ T cells was primary agent of demyelination, whereas IFNγ was not essential for GI dysmotility in WNV-infected mice. Similarly, and despite being implicated in the damage to enteric neurons in a model of ganglionitis (72), TNF was not required for intestinal motility defects in WNV-infected mice. Instead, our T cell depletion studies in KO mice suggest that both perforin and FasL-dependent cytolytic mechanisms contribute to neuronal and glial injury in the GI tract of WNV-infected mice. Our experiments in DKO mice show that both perforin and Fas-ligand-dependent mechanisms contribute to the pathologic changes in the small intestine during WNV infection. Similarly to *TCRbd*$^{-/-}$, we also observed higher levels of WNV Ag in neurons on day 7 post infection in DKO mice. This result, together with our observation of intact neuronal and glial networks, confirms the important role of FasL and perforin as the principal damaging T cell effector mechanisms during the immune response to WNV in the gut.

We acknowledge several limitations of our studies. (a) We used WNV as a model infection to study acute and chronic GI dysmotility of the small intestine, even though a similar syndrome has not been definitively demonstrated in humans. (b) For studies with *TCRbd*$^{-/-}$ mice or animals lacking T cells due to depletion with antibodies, we are limited to evaluating early time points for GI tract motility measurements because these mice succumb to uncontrolled WNV infection in the brain and spinal cord at later time points. (c) Since all neurons in the brain and spinal cord are susceptible to WNV infection, we cannot rule out an impact of CNS dysfunction on the gut motility phenotype. Measurements of peristalsis and GI tract function in isolated intestines from WNV-infected mice might address this problem. (d) Some treatments (*e.g.*, anti-CSF1R antibody) led to dysmotility that lasted more than 6 h; however, we were not able to quantify this effect further

444 due to time limitations in our mouse facility. (e) Our experiments were performed with male and
445 female mice that were randomly assigned to specific experimental groups. While some studies
446 show differences in GI tract motility depending on the sex of the mice or phase of the estrous
447 cycle (73-75), we observed similar phenotypes in male and female mice. However, we did not
448 specifically test for effects of WNV infection on GI tract motility in females at proestrus, estrus,
449 metestrus, or diestrus phases. (f) We observed an imperfect correlation between damage to
450 neurons and glia and GI dysmotility, which might be due to tissue sampling bias. Functional
451 experiments *ex vivo* that stimulate neurons from WNV-infected mice might provide more precise
452 correlations.

453 In summary, our experiments show how the effector functions used by infiltrating antigen
454 specific $CD4^+$ and $CD8^+$ T cells can rapidly injure the neurons and the neighboring glia resulting
455 in durable tissue damage and long-term intestinal transit dysfunction. Pharmacological control of
456 these T cell effector functions may be challenging given the need to prevent sustained neurotropic
457 viral infection that intrinsically can cause damage in the GI tract, and in other tissues, like the brain
458 and spinal cord.

MATERIALS AND METHODS

Sex as a biological variable. Our study examined male and female animals, and similar findings are reported for both sexes.

Mice. Wt C57BL/6J (# 000664), *TCRbd*$^{-/-}$ (B6.129P2-Tcrbtm1Mom/J; # 002122), *Prf1*$^{-/-}$ (C57BL/6-Prf1tm1Sdz/J; # 002407), *FasL*$^{gld/gld}$ (B6Smn.C3-Faslgld/J, # 001021), *Ifngr*$^{-/-}$ (B6.129S7-Ifngr1tm1Agt/J; # 003288), *ChaT* GFP (B6.Cg-Tg(RP23-268L19-EGFP)2Mik/J; # 007902), *Ccr2 GFP* (B6(C)-Ccr2tm1.1Cln/J; # 027619), Ai3 (B6.Cg-Gt(ROSA)26Sortm3(CAG-EYFP)Hze/J; # 007903) and *Rag1*$^{-/-}$ (B6.129S7-*Rag1*^{tm1Mom}/J; # 002216) mice were obtained commercially (Jackson Laboratories). *Snap25l10a* GFP mice (B6;FVB-Tg (Snap25-EGFP/Rpl10a)JD362Htz/J; # 030273; Jackson Laboratories) were kindly provided by Dr. Joseph D. Dougherty (Washington University in St. Louis). *Ccr2* CreER mice were kindly provided by Dr. Burkhard Becher (University of Zurich, Zurich) and crossed to *Ai3* (Rosa26 YFP) to obtain *Ccr2* CreER *Rosa26 YFP*. *DKO* (*Prf1*$^{-/-}$*; Fasl*$^{gld/gld}$) mice were generated by crossing of *Prf*$^{-/-}$ to *Fasl*$^{gld/gld}$. Heterozygous *Prf1*$^{+/-}$*; Fasl*$^{gld/+}$ were mated with *Prf1*$^{-/-}$, and *Prf1*$^{-/-}$ *; Fasl*$^{gld/+}$ were selected for brother-sister matings to obtain DKO mice. All mice were bred under pathogen-free conditions at Washington University School of Medicine.

Nine-to-ten-week-old male or female C57BL6/J mice or transgenic and knockout mice were inoculated with 10^2 focus-forming units (FFU) of WNV in 50 µL of PBS via subcutaneous injection to footpad. All dissections and inoculations were performed under anesthesia, induced and maintained by using ketamine hydrochloride and xylazine or isoflurane and every effort was made to minimize suffering.

Viruses. WNV New York 1999 (clone 382-99 (76) was propagated in Vero cells (passage 1) as described previously (2). Viral stocks were titrated using focus forming assay on Vero WHO cells (2).

GI tract motility measurements. GI tract motility was assessed as described previously (77), briefly, mice were administered with 300 µL of 6% (w/v) carmine red dye (Sigma Aldrich) in

0.5 % methylcellulose diluted in sterile water via oral gavage. After 3 h, mice were placed individually into paper card boxes, and fecal pellets were examined for red color every 5 to 10 min.

Enrichment and adoptive transfer of T cells. Spleens and mesenteric lymph nodes from isoflurane-overdosed WNV-infected (7 dpi) wt or naïve WNV NS4B and LCMV P14 TCR transgenic mice were harvested, and single cell suspensions were obtained by mashing with syringe plunger through a cell strainer (70 μm), followed by lysis of erythrocytes using ACK lysis buffer for 3 min on ice. After washing with PBS + 0.5% BSA + 2 mM EDTA, cells were counted, and the single cell suspension was enriched for $CD4^+$ or $CD8^+$ T cells by negative selection using CD4 or CD8a T cell Isolation Kit (Miltenyi; # 130-104-454 and # 130-104-075) following the manufacturer's instructions. For transfer of WNV NS4B and P14 TCR T cells, *TCRbd*$^{-/-}$ mice were administered 10^6 $CD8^+$ T cells in 100 μL of PBS via retroorbital injection at one day prior to WNV infection. $CD4^+$ (10^7) or $CD8^+$ (5×10^6) T cells were administered via retroorbital injection to *TCRbd*$^{-/-}$ mice 2 days after WNV infection. For each experiment, the efficiency of T cell enrichment and transfer was assessed by flow cytometry.

Statistical analyses. We performed statistical analyses using Prism 9.0. Two-tailed Mann-Whitney, one-way Kruskal-Wallis ANOVA with Dunn's correction, one-way ANOVA with Dunnet's correction, and Chi-squared test with Bonferroni correction were used to determine significance depending on the number of comparison groups and the data variance. Details of statistical tests used are included in the Figure Legends.

Study approval. This study was conducted in accordance with the recommendations of the Guide for the Care and Use of Laboratory Animals of the National Institutes of Health. Animal experiments were performed as specified in protocols approved by the Institutional Animal Care and Use Committee at the Washington University School of Medicine (Assurance Number: A3381-01).

Data availability. Data are available from the corresponding author upon request. All data supporting the graphs are provided in the **Supplemental Supporting Data Values** XLS file. RNAseq data generated in this study have been deposited in the GEO database with accession code GSE264415.

AUTHOR CONTRIBUTIONS

H.J. performed all mouse treatments and infections, tissue harvesting, flow cytometry, confocal imaging, gut motility assays and analysis. F.R.Z. and P.D. performed tissue harvesting, flow cytometry, and RNA-seq analysis and helped with experimental design. M.M. provided anti-CCR2 mAb. H.J., L.B.T., T.S.S. and M.S.D. designed experimental studies and analyzed results. H.J., T.S.S., and M.S.D. wrote the initial draft, with all other authors providing editorial comments.

ACKNOWLEDGEMENTS

We thank Miriam Medina Fernandes and Michelle Elam-Noll posthumously for their assistance with mouse husbandry. We acknowledge Dr. Wandy L. Beatty in the Washington University Molecular Microbiology Imaging Facility for assistance with confocal imaging. This study was supported by a grant from the NIH (R01 DK122790) to T.S.S. and M.S.D. Some of the figures (Figure 1 and 7; Supplementary Figures 1, 3, 4, 5, and 6; and the Graphical Abstract) were created using BioRender software.

MAIN FIGURE LEGENDS

Figure 1. WNV infection induces changes in ENS neuronal networks. (**A**) Timeline of WNV infection. 9 to 10-week-old C57BL6/J male mice were inoculated in the footpad with 10^2 FFU of WNV (New York 1999 strain), and carmine dye transit assay and tissue collections were performed at indicated time points. (**B-C**) Whole mount preparations of the muscularis externa from *ChAT*-eGFP reporter mice were isolated at 5 or 6 dpi and co-stained for WNV antigen, calretinin$^+$ and nNOS$^+$ neurons. (**B**) Blue, green, and white arrows indicate WNV antigen$^+$ calretinin$^+$ neurons, ChAT$^+$ neurons, and nNOS$^+$ neurons, respectively. Images are representative of 2 experiments; scale bar, 50 μm. (**C**) The proportion of specific neuronal subgroups infected with WNV. (**D**) Percentage of mice having WNV antigen in the proximal, middle (mid), and distal regions of small intestine (SI) at 6 dpi. (**E-K**) Muscularis externa with the attached layer containing submucosal plexus (SMP) (**G**), myenteric plexus (MP) (**F, I-K**), or with MP only or both MP and SMP, as indicated (**E**, **H**) was isolated from the mid and distal SI of sham or WNV-infected mice at 7 dpi (**E-H**) or 15, 28, and 65 dpi (**I-K**) and stained for neuronal markers. (**E, I**) The total number of HuC/D$^+$ neurons in (**E**) submucosal (SMP) and myenteric plexus (MP) or (**I**) MP only was counted and is shown as number of neurons per mm^2. (**F-G**) The fraction of area staining positive for nNOS, calretinin, and 5-HT in the MP (**F**) or calretinin in the SMP (**G**) was determined, and the values were normalized to sham-infected mice. Circles, squares, and triangles indicate nNOS$^+$, calretinin$^+$, and 5-HT$^+$ neurons, respectively. (**H**) Representative images show staining for indicated markers in mid SI in sham and WNV-infected mice at 7 dpi in either MP or SMP as indicated. Scale bar, 100 μm. (**J**) nNOS$^+$ and calretinin$^+$, and (**K**) 5-HT$^+$ cell area was determined, and the values were normalized to sham-infected mice. (**I-K**) Representative images show staining in mid SI in sham and WNV-infected mice at 65 dpi. Scale bar, 100 μm. (**L-O**) Analysis of neuron-specific RNA sequencing using TRAP in WNV or mock-infected *Snap25I10a* mice 6 dpi. (**L**) Principal component analysis (PCA). (**M**) Volcano plot of differential expression analysis (DEseq2) of Translating Ribosome Affinity Purification (TRAP)-seq comparing WNV and mock-

infected samples. Red dots indicate log_2 fold-change > 1, and FDR (p adjusted) < 0.05 while blue dots indicate log_2 fold-change < -1 and p adjusted < 0.05. (**N-O**) Heatmap of differentially expressed genes in sham and WNV-infected mice showing genes related to (**N**) response to virus, and (**O**) cytokines and chemokines. Expression levels are normalized across each gene and represent the average of 4 mice per condition. Data are pooled from the following number of experiments: (**C-D**) 2; (**E-K**) 3 (MP) or 2 (SMP); (**F**) 3; (**G**) 2, (**I**) 3; (**J**) 2 (15 dpi), 3 (28 dpi), or 4 (65 dpi); (**K**) 2 (15 dpi), 3 (28 dpi), or 2 (65 dpi). The indicated numbers of mice per group were used (left to right): (**C**) 6, 6, 6; (**D**) 9, 9, 9; (**E**) 9, 9, 11, 11, 7, 8, 7, 7; (**F**) 9, 9, 9, 9, 9, 9, 9, 9, 6, 6, 10, 8; (**G**) 7, 7, 6, 7; (**I**) 10, 9, 10, 13, 13, 13, 13, 13, 13, 14, 16, 14, 16; (**J**) 8, 8, 8, 8, 10, 9, 10, 10, 12, 13, 12, 13, 8, 8, 8, 8, 10, 10, 10, 9, 12, 13, 12, 13; (**K**) 5, 7, 5, 7, 9, 10, 10, 10, 5, 7, 5, 7. (**C, E-G, I-K**) Column heights indicate mean values. Statistical analysis: two-tailed Mann-Whitney test: not significant, ns, *p < 0.05, **p < 0.01, ***p < 0.001.

Figure 2. WNV infection affects enteric glial networks. (**A-C**) Muscularis externa was isolated from mid and distal regions of small intestine (SI) of sham or WNV-infected C57BL/6J mice at (**A-B**) 7 dpi or (**C**) 15, 28, and 65 dpi and stained for glia (S100β). The fraction of area staining positive for S100β was determined, and the values were normalized to sham-infected mice. Representative images show S100β staining in the mid region of SI in sham and WNV-infected mice at 7 (**A**) or 65 (**C**) dpi; scale bar, 100 μm Data are pooled from (**A**, **B**) 2 experiments, n = 5-10 per group; (**C)** from left to right: 2, 3, 4 experiments, n = 6-10, 12-13, 13-16. Column heights indicate mean values. Statistical analysis: two-tailed Mann-Whitney test: not significant, ns, *p < 0.05, **p < 0.01, ***p < 0.001.

Figure 3. WNV infection promotes infiltration of monocytes into the intestine. (**A-E**) Whole mount preparations of the muscularis externa were isolated from the middle and distal regions of small intestine (SI) of WNV-infected heterozygous *Ccr2*-GFP mice at (**A, B**) 6 or (**C**) 15 dpi and stained for (**A**) neuron (HuC/D) and macrophage (Iba1) markers, (**B**) WNV antigen and macrophage markers, or (**C-E**) macrophage markers. Yellow arrows indicate monocytes (CCR2

582 GFP$^+$ Iba1$^-$ cells). Scale bar, 100 μm. (**A-C**) Representative images are obtained from the
583 myenteric plexus of the mid region of SI from at least 2 experiments. (**D**) Monocytes (*Ccr2* GFP$^+$
584 Iba1$^-$) in the myenteric plexus are shown as the numbers of cells per mm^2. (**E**) The fraction of
585 *Ccr2* GFP-positive area (representing monocytes and/or monocyte-derived macrophages) in the
586 myenteric plexus of WNV- or sham-infected mice. (**F-G**) Muscularis externa of mid and distal SI
587 from sham or WNV-infected mice harvested at 15, 28, or 65 dpi were stained for macrophages
588 (Iba1). Macrophages in (**F**) the myenteric plexus and (**G**) the circular muscle layer are shown as
589 the number of Iba1$^+$ cells per mm^2. Images are representative of Iba1 staining in sham or WNV-
590 infected mice at 65 dpi. Scale bar, 100 μm. (**H-J**) GI transit was measured after oral gavage of
591 carmine red dye (**H**) in sham or WNV-infected mice (at 7 dpi) after treatment with anti-CCR2 or
592 isotype mAbs, (**I**) in WNV-infected *Ccr2*$^{+/-}$ and *Ccr2*$^{-/-}$ mice, (**J**) in sham or WNV-infected mice after
593 treatment with anti-CSF1R or isotype control mAb. (**K-M**). Whole mount preparations of the
594 muscularis externa were isolated from the middle region of SI of WNV-infected mice treated with
595 anti-CSF1R or isotype mAbs and stained for (**K**) nNOS$^+$ and calretinin$^+$ neurons, (**L**) 5-HT$^+$
596 neurons or (**M**) S100β$^+$ glia. Scale bar, 100 μm. The fraction of area staining positive for calretinin,
597 nNOS, 5-HT or S100β was determined, and values were normalized to sham-infected mice
598 treated with isotype control mAb. Data are pooled from: (**D, E**) 2, (**F, G**) 2 (15 dpi), 3 (28 dpi), 4
599 (65 dpi); (**H**) 3; (**I**) 1; (**J**) 3; (**K-M**) 3 experiments with indicated numbers of mice per group (from
600 left to right): (**D, E**) 4, 7, 4, 7; (**F**) 9, 10, 10, 10, 13, 13, 13, 11, 11, 12, 11; (**G**) 10, 10, 10, 10, 12,
601 12, 11, 12, 12, 11, 11, 11; (**H**) 5, 5, 20, 15; (**I**) 7,10; (**J**) 9, 7, 16, 15; (**K**) 7, 6, 13, 12; (**L**) 5, 5, 10,10;
602 and (**M**) 7, 7, 13, 12. (**D-G** and **J-L**). Column height indicates mean values. (**H-J**) Lines indicate
603 median values. Statistical analysis: (**D, F-G**) Two-tailed Mann-Whitney test; (**L**) Kruskal-Wallis
604 ANOVA with Dunn's post-test. Not significant, ns, *p < 0.05, **p < 0.01, ***p < 0.001, ****p <
605 0.0001.

606 **Figure 4. Damage to neuronal and glial network is caused by CD4$^+$ and CD8$^+$ T cells.**
607 (**A, F**) GI transit was measured after oral gavage of carmine red dye. (**A**) Transit time in sham or

WNV-infected wt or *TCRbd*$^{-/-}$ mice at 7 dpi. (**B, C, D, G, H**). Muscularis externa was isolated from (**B, C, D**) middle and distal regions of small intestine (SI) of sham or WNV-infected wt or *TCRbd*$^{-/-}$ mice at 7 dpi, (**G, H**) middle regions of SI sham or WNV-infected wt mice at 7 dpi treated with anti-CD4 and/or anti-CD8β or isotype control mAbs and stained for (**B, G**) calretinin^{+} and nNOS^{+} neurons, (**C**) WNV antigen, (**D**) S100β^{+} glia, or (**H**) and S100β^{+} glia and WNV antigen. The fraction of area staining positive for calretinin, nNOS or S100β was determined, and the values were normalized to (**B, D**) wt sham-infected mice or (**G-H**) animals treated with isotype control mAb. Representative images from the myenteric plexus of the middle region of SI, scale bar, 100 μm. (**C**) Data are presented as the percentage of WNV antigen-positive area in the field of view. (**E**) Counts of live CD45^{+} TCRβ^{+} CD4^{+} or CD8^{+} T cells in muscularis of sham or WNV-infected C57BL6/J mice at 7 dpi. (**F**) Transit time of sham or WNV-infected mice at 7 dpi treated with anti-CD4 and/or anti-CD8β or isotype control mAbs. Data are pooled from (**A**) 3; (**C-E, G**) 2; and (**F**) 4 experiments with indicated numbers of mice per group (left to right): (**A**) 7, 7, 13, 12; (**C-D**) 5, 5, 8, 7; (**E**) 6, 6, 7, 7; (**F**) 8, 18, 10, 10, 18; (**G)** 8, 7, 8, 7, 8, 8; (**H**) 6, 7, 8. (**A, E, F**) Lines indicate the mean values. (**B, C, D, G, H**) Column height indicates mean values. Statistical analysis: (**A**, **B, D, G, H**) Kruskal-Wallis ANOVA with Dunn's post-test (all groups compared to each other); (**F**) Kruskal-Wallis ANOVA with Dunn's post-test (comparison to "isotype control" group); and (**C**) two-tailed Mann-Whitney test: not significant, ns, *$p < 0.05$, **$p < 0.01$, ***$p < 0.001$.

Figure 5. Damage to neuronal and glial network is caused by WNV-specific CD8^{+} and CD4^{+} T cells. (**A-E**) Adoptive transfer of WNV-primed wt CD4^{+} or CD8^{+} T cells to *TCRbd*$^{-/-}$ mice. CD4^{+} or CD8^{+} T cells from WNV-infected wt mice were isolated at 7 dpi and adoptively transferred to *TCRbd*$^{-/-}$ at 2 dpi. (**A**) GI transit time in recipient *TCRbd*$^{-/-}$ mice at 7 dpi, (**B**) proportions of mice with severe GI dysmotility ($\geq$ 360 min), (**C-D**) analysis of neuronal (calretinin, nNOS) and glial (S100β) networks from middle small intestine (SI) at 7 dpi, and (**E**) representative images obtained from the myenteric plexus of the middle region of SI, scale bar, 100 μm. (**F**) Flow cytometric analysis of muscularis externa or mucosa and lamina propria at 7 dpi. Cells were

stained with mAbs to CD45, TCRβ, TCRγδ, CD8a, CD44, and WNV NS4B D^b-restricted tetramers and gated on live $CD45^+$ $TCR\beta^+$ $CD8^+$ cells (see **Fig S4C**). Graph shows percentage of $CD8^+$T cells positive for NS4B. (**G-I**) Adoptive transfer of $CD8^+$ T cells from P14 transgenic mice (targeting LCMV gp33 peptide) or WNV NS4B transgenic mice to *TCRbd*$^{-/-}$ mice. T cells were administered to *TCRbd*$^{-/-}$ mice one day prior to subcutaneous inoculation with WNV. (**G**) GI transit 7 dpi, (**H-I**) analysis of neuronal (calretinin, nNOS) and glial network (S100β) from mid and distal SI at 7 dpi. (**A, G**) GI transit was measured after oral gavage of carmine red dye. (**C, D, H, I**) The fraction of area positive for calretinin, nNOS or S100β was determined, and values were normalized to (**C, D**) wt sham mice or (**H, I**) *TCRbd*$^{-/-}$ mice without adoptive transfer. Data are pooled from, (**A, B, C, D**) 6; (**F**) 2; and (**G-I**) 3 experiments with indicated numbers of mice per group (left to right): (**F**) 6; (**A**) 13, 12, 9, 13, 8; (**B**) 9, 13, 8; (**C, D**) 11, 9, 13, 8; (**F**) 6, 6; (**G**) 5, 8, 9; (**H, I**) 6, 8, 10, 6, 8, 10. Lines indicate (**G, F**) median and column heights indicate (**C, D, H, I**) mean values. Statistical analysis: (**C, D**) ANOVA with Dunnett's post-test (comparison to "no transfer" group); (**B**) Chi-squared test with Bonferroni correction (proportions compared to "no transfer" group); and (**G-I**) Kruskal-Wallis ANOVA with Dunn's post-test (comparison to "no transfer" group): not significant, ns, *$p < 0.05$, **$p < 0.01$.

Figure 6. $CD4^+$ and $CD8^+$ T cells injure neurons and glia using multiple effector functions. (**A, B, C, D, H, K**) GI tract transit was measured after oral gavage of carmine red dye at 7 dpi. Transit time of sham, WNV-infected wild-type (*WT*) or WNV-infected (**A**) *Prf1*$^{-/-}$ mice, (**B**) *Fasl*$^{gld/gld}$ mice, (**C**) *Ifngr*$^{-/-}$ mice, (**D**) wt mice treated with anti-TNF or isotype control mAb or WNV-infected, (**H**) *Prf1*$^{-/-}$ mice or (**K**) *Fasl*$^{gld/gld}$ mice treated with anti-CD4, anti-CD8β or isotype control mAb. (**E, F, I, J, L**) Muscularis externa was isolated from mid regions of small intestine (SI) of sham, WNV-infected wt or *Prf1*$^{-/-}$ (**E**), *Fasl*$^{gld/gld}$ (**F**) or WNV-infected *Prf1*$^{-/-}$ (**I, J**) or *Fasl*$^{gld/gld}$ (**L**) mice treated with anti-CD4 or anti-CD8β mAb at 7 dpi and stained. The fraction of positive area for calretinin, nNOS or S100β was determined, and values were normalized to sham-infected wt

mice. (**J**) Representative images are obtained from the myenteric plexus of the middle region of the SI, scale bar 100 μm. Data are pooled from: (**A, B, C, F, I, J**) 3; (**D, G, L**) 2; (**E, K**) 5; and (**H**) 4 experiments with indicated numbers of mice per group (left to right): (**A**) 4, 4, 5, 11; (**B**) 9, 7, 10, 9; (**C**) 7, 4, 9, 11; (**D**) 10, 10; (**E**) 13, 4, 7, 12, 13, 4, 7, 12, 10, 4, 7, 11; (**F**) 11, 7, 11, 8, 10, 7, 10, 8, 11, 7, 11, 8 6; (**G**) 6, 6; (**H**) 12, 9, 12; (**I**) 12, 9, 12, 9, 11, 9; (**K**) 15, 7, 13; (**L**) 7, 6, 7, 6, 7, 6. Lines indicate (**A-D, G**) median or (**H, K**) mean. Column heights indicate mean values. Statistical analysis: (**A-F, I, L**) Mann-Whitney test; (**H, K**) ANOVA with Dunnett's post-test (comparison to "isotype control" group): not significant, ns, *p < 0.05, **p < 0.01.

Figure 7. Mice lacking perforin and Fas-FasL signaling do not develop WNV-triggered GI dysmotility or neuronal and glial network injury. (**A**) Scheme of generation of *Prf1*$^{-/-}$*; Fasl*$^{gld/gld}$ (DKO) mice. (**B**) GI transit time in WNV-infected wt or DKO mice at 7 dpi. (**C**) Proportions of WNV-infected wt and DKO mice showing abnormal bowel dilation in the small intestine (SI) at 7 dpi. (**D-G**) Muscularis externa was isolated from middle regions of SI of sham (**D, E**) or WNV-infected wt or DKO (**F, G**) mice at 7 dpi and stained. (**D-F**) The fraction of positive area for calretinin, nNOS, S100β, and WNV antigen was determined, and values were normalized to (**D, E**) sham-infected wt mice or (**F**) to WNV-infected wt mice. (**G**) Numbers of $CD3^+$ cells in the myenteric plexus were calculated by dividing the area positive for $CD3^+$ staining with average size of $CD3^+$ cell. Cell counts are expressed as numbers of $CD3^+$ cells per mm^2. (**D, G**) Representative images are obtained from the myenteric plexus of the middle region of small intestine, scale bar 100 μm. Data are pooled from: (**B, C, F**) 5 and (**D, E, G**) 4 experiments with indicated numbers of mice per group (left to right): (**B, C**) 16, 13; (**D, E**) 10, 8, 10; (**F**) 15, 10; and (**G**) 10, 10. (**B**) Lines and (**D-G**) column heights indicate mean values. Statistical analysis: (**B, F, G**) Two-tailed Mann-Whitney test; (**D, E**) Kruskal-Wallis ANOVA with Dunn's post-test. Not significant, ns, *p < 0.05, **p < 0.01, ***p < 0.001.

REFERENCES

1. Spencer NJ, and Hu H. Enteric nervous system: sensory transduction, neural circuits and gastrointestinal motility. *Nat Rev Gastroenterol Hepatol.* 2020;17(6):338-51.
2. White JP, Xiong S, Malvin NP, Khoury-Hanold W, Heuckeroth RO, Stappenbeck TS, et al. Intestinal Dysmotility Syndromes following Systemic Infection by Flaviviruses. *Cell.* 2018;175(5):1198-212 e12.
3. Klein S, Seidler B, Kettenberger A, Sibaev A, Rohn M, Feil R, et al. Interstitial cells of Cajal integrate excitatory and inhibitory neurotransmission with intestinal slow-wave activity. *Nat Commun.* 2013;4:1630.
4. Rao M, Rastelli D, Dong L, Chiu S, Setlik W, Gershon MD, et al. Enteric Glia Regulate Gastrointestinal Motility but Are Not Required for Maintenance of the Epithelium in Mice. *Gastroenterology.* 2017;153(4):1068-81.e7.
5. Muller PA, Matheis F, and Mucida D. Gut macrophages: key players in intestinal immunity and tissue physiology. *Curr Opin Immunol.* 2020;62:54-61.
6. Mawe GM. Colitis-induced neuroplasticity disrupts motility in the inflamed and post-inflamed colon. *J Clin Invest.* 2015;125(3):949-55.
7. Musser MA, Correa H, and Southard-Smith EM. Enteric neuron imbalance and proximal dysmotility in ganglionated intestine of the Sox10(Dom/+) Hirschsprung mouse model. *Cell Mol Gastroenterol Hepatol.* 2015;1(1):87-101.
8. Sanders KM, Drumm BT, Cobine CA, and Baker SA. Ca(2+) dynamics in interstitial cells: foundational mechanisms for the motor patterns in the gastrointestinal tract. *Physiol Rev.* 2024;104(1):329-98.
9. Forootan M, Bagheri N, and Darvishi M. Chronic constipation: A review of literature. *Medicine (Baltimore).* 2018;97(20):e10631.
10. Sperber AD, Bangdiwala SI, Drossman DA, Ghoshal UC, Simren M, Tack J, et al. Worldwide Prevalence and Burden of Functional Gastrointestinal Disorders, Results of Rome Foundation Global Study. *Gastroenterology.* 2021;160(1):99-114 e3.
11. Beatty JK, Bhargava A, and Buret AG. Post-infectious irritable bowel syndrome: mechanistic insights into chronic disturbances following enteric infection. *World J Gastroenterol.* 2014;20(14):3976-85.
12. Matheis F, Muller PA, Graves CL, Gabanyi I, Kerner ZJ, Costa-Borges D, et al. Adrenergic Signaling in Muscularis Macrophages Limits Infection-Induced Neuronal Loss. *Cell.* 2020;180(1):64-78 e16.
13. Khoury-Hanold W, Yordy B, Kong P, Kong Y, Ge W, Szigeti-Buck K, et al. Viral Spread to Enteric Neurons Links Genital HSV-1 Infection to Toxic Megacolon and Lethality. *Cell Host Microbe.* 2016;19(6):788-99.
14. Brun P, Qesari M, Marconi PC, Kotsafti A, Porzionato A, Macchi V, et al. Herpes Simplex Virus Type 1 Infects Enteric Neurons and Triggers Gut Dysfunction via Macrophage Recruitment. *Frontiers in Cellular and Infection Microbiology.* 2018;8.
15. Diamond MS, Shrestha B, Marri A, Mahan D, and Engle M. B cells and antibody play critical roles in the immediate defense of disseminated infection by West Nile encephalitis virus. *J Virol.* 2003;77(4):2578-86.
16. Sharkey KA, and Mawe GM. The enteric nervous system. *Physiol Rev.* 2023;103(2):1487-564.
17. Cairns BR, Jevans B, Chanpong A, Moulding D, and McCann CJ. Automated computational analysis reveals structural changes in the enteric nervous system of nNOS deficient mice. *Sci Rep.* 2021;11(1):17189.
18. Belkind-Gerson J, Hotta R, Nagy N, Thomas AR, Graham H, Cheng L, et al. Colitis induces enteric neurogenesis through a 5-HT4-dependent mechanism. *Inflamm Bowel Dis.* 2015;21(4):870-8.

19. Shah PA, Park CJ, Shaughnessy MP, and Cowles RA. Serotonin as a Mitogen in the Gastrointestinal Tract: Revisiting a Familiar Molecule in a New Role. *Cell Mol Gastroenterol Hepatol.* 2021;12(3):1093-104.
20. Seguella L, and Gulbransen BD. Enteric glial biology, intercellular signalling and roles in gastrointestinal disease. *Nature Reviews Gastroenterology & Hepatology.* 2021;18(8):571-87.
21. Drokhlyansky E, Smillie CS, Van Wittenberghe N, Ericsson M, Griffin GK, Eraslan G, et al. The Human and Mouse Enteric Nervous System at Single-Cell Resolution. *Cell.* 2020;182(6):1606-22 e23.
22. Zeisel A, Hochgerner H, Lonnerberg P, Johnsson A, Memic F, van der Zwan J, et al. Molecular Architecture of the Mouse Nervous System. *Cell.* 2018;174(4):999-1014 e22.
23. Laranjeira C, Sandgren K, Kessaris N, Richardson W, Potocnik A, Vanden Berghe P, et al. Glial cells in the mouse enteric nervous system can undergo neurogenesis in response to injury. *J Clin Invest.* 2011;121(9):3412-24.
24. Belkind-Gerson J, Graham HK, Reynolds J, Hotta R, Nagy N, Cheng L, et al. Colitis promotes neuronal differentiation of Sox2+ and PLP1+ enteric cells. *Sci Rep.* 2017;7(1):2525.
25. Guyer RA, Stavely R, Robertson K, Bhave S, Mueller JL, Picard NM, et al. Single-cell multiome sequencing clarifies enteric glial diversity and identifies an intraganglionic population poised for neurogenesis. *Cell Rep.* 2023;42(3):112194.
26. Sanders KM, Ward SM, and Koh SD. Interstitial cells: regulators of smooth muscle function. *Physiol Rev.* 2014;94(3):859-907.
27. Brun P, Giron MC, Zoppellaro C, Bin A, Porzionato A, De Caro R, et al. Herpes simplex virus type 1 infection of the rat enteric nervous system evokes small-bowel neuromuscular abnormalities. *Gastroenterology.* 2010;138(5):1790-801.
28. Guilliams M, Mildner A, and Yona S. Developmental and Functional Heterogeneity of Monocytes. *Immunity.* 2018;49(4):595-613.
29. Avetisyan M, Rood JE, Huerta Lopez S, Sengupta R, Wright-Jin E, Dougherty JD, et al. Muscularis macrophage development in the absence of an enteric nervous system. *Proc Natl Acad Sci U S A.* 2018;115(18):4696-701.
30. Mack M, Cihak J, Simonis C, Luckow B, Proudfoot AE, Plachý J, et al. Expression and characterization of the chemokine receptors CCR2 and CCR5 in mice. *J Immunol.* 2001;166(7):4697-704.
31. Bai F, Kong KF, Dai J, Qian F, Zhang L, Brown CR, et al. A paradoxical role for neutrophils in the pathogenesis of West Nile virus. *J Infect Dis.* 2010;202(12):1804-12.
32. Suthar MS, Diamond MS, and Gale M, Jr. West Nile virus infection and immunity. *Nat Rev Microbiol.* 2013;11(2):115-28.
33. Paul AM, Acharya D, Duty L, Thompson EA, Le L, Stokic DS, et al. Osteopontin facilitates West Nile virus neuroinvasion via neutrophil "Trojan horse" transport. *Sci Rep.* 2017;7(1):4722.
34. Lim JK, Obara CJ, Rivollier A, Pletnev AG, Kelsall BL, and Murphy PM. Chemokine receptor Ccr2 is critical for monocyte accumulation and survival in West Nile virus encephalitis. *J Immunol.* 2011;186(1):471-8.
35. Belz GT, Smith CM, Eichner D, Shortman K, Karupiah G, Carbone FR, et al. Cutting edge: conventional CD8 alpha+ dendritic cells are generally involved in priming CTL immunity to viruses. *J Immunol.* 2004;172(4):1996-2000.
36. Shrestha B, and Diamond MS. Role of CD8+ T cells in control of West Nile virus infection. *J Virol.* 2004;78(15):8312-21.
37. Sitati EM, and Diamond MS. CD4+ T-cell responses are required for clearance of West Nile virus from the central nervous system. *J Virol.* 2006;80(24):12060-9.

38. Netland J, and Bevan MJ. CD8 and CD4 T cells in west nile virus immunity and pathogenesis. *Viruses.* 2013;5(10):2573-84.
39. Wang T, Gao Y, Scully E, Davis CT, Anderson JF, Welte T, et al. Gamma delta T cells facilitate adaptive immunity against West Nile virus infection in mice. *J Immunol.* 2006;177(3):1825-32.
40. Wang T, Scully E, Yin Z, Kim JH, Wang S, Yan J, et al. IFN-gamma-producing gamma delta T cells help control murine West Nile virus infection. *J Immunol.* 2003;171(5):2524-31.
41. Rahemtulla A, Fung-Leung WP, Schilham MW, Kundig TM, Sambhara SR, Narendran A, et al. Normal development and function of CD8+ cells but markedly decreased helper cell activity in mice lacking CD4. *Nature.* 1991;353(6340):180-4.
42. Tyznik AJ, Sun JC, and Bevan MJ. The CD8 population in CD4-deficient mice is heavily contaminated with MHC class II-restricted T cells. *J Exp Med.* 2004;199(4):559-65.
43. Kim TS, and Shin EC. The activation of bystander CD8(+) T cells and their roles in viral infection. *Exp Mol Med.* 2019;51(12):1-9.
44. Purtha WE, Myers N, Mitaksov V, Sitati E, Connolly J, Fremont DH, et al. Antigen-specific cytotoxic T lymphocytes protect against lethal West Nile virus encephalitis. *Eur J Immunol.* 2007;37(7):1845-54.
45. Kim S, Pinto AK, Myers NB, Hawkins O, Doll K, Kaabinejadian S, et al. A novel T-cell receptor mimic defines dendritic cells that present an immunodominant West Nile virus epitope in mice. *Eur J Immunol.* 2014;44(7):1936-46.
46. Aguilar-Valenzuela R, Netland J, Seo YJ, Bevan MJ, Grakoui A, and Suthar MS. Dynamics of Tissue-Specific CD8(+) T Cell Responses during West Nile Virus Infection. *J Virol.* 2018;92(10).
47. Pircher H, Moskophidis D, Rohrer U, Burki K, Hengartner H, and Zinkernagel RM. Viral escape by selection of cytotoxic T cell-resistant virus variants in vivo. *Nature.* 1990;346(6285):629-33.
48. Shrestha B, and Diamond MS. Fas ligand interactions contribute to CD8+ T-cell-mediated control of West Nile virus infection in the central nervous system. *J Virol.* 2007;81(21):11749-57.
49. Shrestha B, Samuel MA, and Diamond MS. CD8+ T cells require perforin to clear West Nile virus from infected neurons. *J Virol.* 2006;80(1):119-29.
50. Shrestha B, Zhang B, Purtha WE, Klein RS, and Diamond MS. Tumor necrosis factor alpha protects against lethal West Nile virus infection by promoting trafficking of mononuclear leukocytes into the central nervous system. *J Virol.* 2008;82(18):8956-64.
51. Diamond MS, and Gale M, Jr. Cell-intrinsic innate immune control of West Nile virus infection. *Trends Immunol.* 2012;33(10):522-30.
52. Shrestha B, Pinto AK, Green S, Bosch I, and Diamond MS. CD8+ T cells use TRAIL to restrict West Nile virus pathogenesis by controlling infection in neurons. *J Virol.* 2012;86(17):8937-48.
53. Ruuls SR, Hoek RM, Ngo VN, McNeil T, Lucian LA, Janatpour MJ, et al. Membrane-bound TNF supports secondary lymphoid organ structure but is subservient to secreted TNF in driving autoimmune inflammation. *Immunity.* 2001;15(4):533-43.
54. Cenerenti M, Saillard M, Romero P, and Jandus C. The Era of Cytotoxic CD4 T Cells. *Frontiers in Immunology.* 2022;13.
55. Brien JD, Uhrlaub JL, and Nikolich-Zugich J. West Nile virus-specific CD4 T cells exhibit direct antiviral cytokine secretion and cytotoxicity and are sufficient for antiviral protection. *J Immunol.* 2008;181(12):8568-75.
56. Hassin D, Garber OG, Meiraz A, Schiffenbauer YS, and Berke G. Cytotoxic T lymphocyte perforin and Fas ligand working in concert even when Fas ligand lytic action is still not detectable. *Immunology.* 2011;133(2):190-6.

57. McClain JL, Fried DE, and Gulbransen BD. Agonist-evoked Ca(2+) signaling in enteric glia drives neural programs that regulate intestinal motility in mice. *Cell Mol Gastroenterol Hepatol.* 2015;1(6):631-45.
58. Ahmadzai MM, Seguella L, and Gulbransen BD. Circuit-specific enteric glia regulate intestinal motor neurocircuits. *Proc Natl Acad Sci U S A.* 2021;118(40).
59. Pochard C, Coquenlorge S, Freyssinet M, Naveilhan P, Bourreille A, Neunlist M, et al. The multiple faces of inflammatory enteric glial cells: is Crohn's disease a gliopathy? *Am J Physiol Gastrointest Liver Physiol.* 2018;315(1):G1-G11.
60. Grundmann D, Loris E, Maas-Omlor S, and Schafer KH. Enteric Neurogenesis During Life Span Under Physiological and Pathophysiological Conditions. *Anat Rec (Hoboken).* 2019;302(8):1345-53.
61. D'Errico F, Goverse G, Dai Y, Wu W, Stakenborg M, Labeeuw E, et al. Estrogen receptor beta controls proliferation of enteric glia and differentiation of neurons in the myenteric plexus after damage. *Proc Natl Acad Sci U S A.* 2018;115(22):5798-803.
62. Soret R, Schneider S, Bernas G, Christophers B, Souchkova O, Charrier B, et al. Glial Cell-Derived Neurotrophic Factor Induces Enteric Neurogenesis and Improves Colon Structure and Function in Mouse Models of Hirschsprung Disease. *Gastroenterology.* 2020;159(5):1824-38.e17.
63. Spencer NJ, and Keating DJ. Role of 5-HT in the enteric nervous system and enteroendocrine cells. *Br J Pharmacol.* 2022.
64. Grainger JR, Konkel JE, Zangerle-Murray T, and Shaw TN. Macrophages in gastrointestinal homeostasis and inflammation. *Pflugers Arch.* 2017;469(3-4):527-39.
65. Zigmond E, Varol C, Farache J, Elmaliah E, Satpathy AT, Friedlander G, et al. Ly6C hi monocytes in the inflamed colon give rise to proinflammatory effector cells and migratory antigen-presenting cells. *Immunity.* 2012;37(6):1076-90.
66. Ahrends T, Aydin B, Matheis F, Classon CH, Marchildon F, Furtado GC, et al. Enteric pathogens induce tissue tolerance and prevent neuronal loss from subsequent infections. *Cell.* 2021;184(23):5715-27 e12.
67. Feng X, Ji Y, Zhang C, Jin T, Li J, and Guo J. CCL6 promotes M2 polarization and inhibits macrophage autophagy by activating PI3-kinase/Akt signalling pathway during skin wound healing. *Exp Dermatol.* 2023;32(4):403-12.
68. Welsh RM, McNally JM, Brehm MA, and Selin LK. Consequences of cross-reactive and bystander CTL responses during viral infections. *Virology.* 2000;270(1):4-8.
69. Whiteside SK, Snook JP, Williams MA, and Weis JJ. Bystander T Cells: A Balancing Act of Friends and Foes. *Trends Immunol.* 2018;39(12):1021-35.
70. Templeton SP, and Perlman S. Pathogenesis of acute and chronic central nervous system infection with variants of mouse hepatitis virus, strain JHM. *Immunol Res.* 2007;39(1-3):160-72.
71. Wu GF, Dandekar AA, Pewe L, and Perlman S. CD4 and CD8 T cells have redundant but not identical roles in virus-induced demyelination. *J Immunol.* 2000;165(4):2278-86.
72. Sanchez-Ruiz M, Iorgu AM, Kuster F, Hellmich M, Brunn A, and Deckert M. CD8 T cell-Derived Perforin and TNF-alpha Are Crucial Mediators of Neuronal Destruction in Experimental Autoimmune Enteric Ganglionitis. *Am J Pathol.* 2021;191(6):1064-76.
73. Balasuriya GK, Nugapitiya SS, Hill-Yardin EL, and Bornstein JC. Nitric Oxide Regulates Estrus Cycle Dependent Colonic Motility in Mice. *Front Neurosci.* 2021;15:647555.
74. Rastelli D, Robinson A, Lagomarsino VN, Matthews LT, Hassan R, Perez K, et al. Diminished androgen levels are linked to irritable bowel syndrome and cause bowel dysfunction in mice. *J Clin Invest.* 2022;132(2).
75. Balasuriya GK, Hill-Yardin EL, Gershon MD, and Bornstein JC. A sexually dimorphic effect of cholera toxin: rapid changes in colonic motility mediated via a 5-HT3 receptor-dependent pathway in female C57Bl/6 mice. *J Physiol.* 2016;594(15):4325-38.

76. Beasley DW, Whiteman MC, Zhang S, Huang CY, Schneider BS, Smith DR, et al. Envelope protein glycosylation status influences mouse neuroinvasion phenotype of genetic lineage 1 West Nile virus strains. *J Virol.* 2005;79(13):8339-47.
77. Desai P, Janova H, White JP, Reynoso GV, Hickman HD, Baldridge MT, et al. Enteric helminth coinfection enhances host susceptibility to neurotropic flaviviruses via a tuft cell-IL-4 receptor signaling axis. *Cell.* 2021;184(5):1214-31.e16.

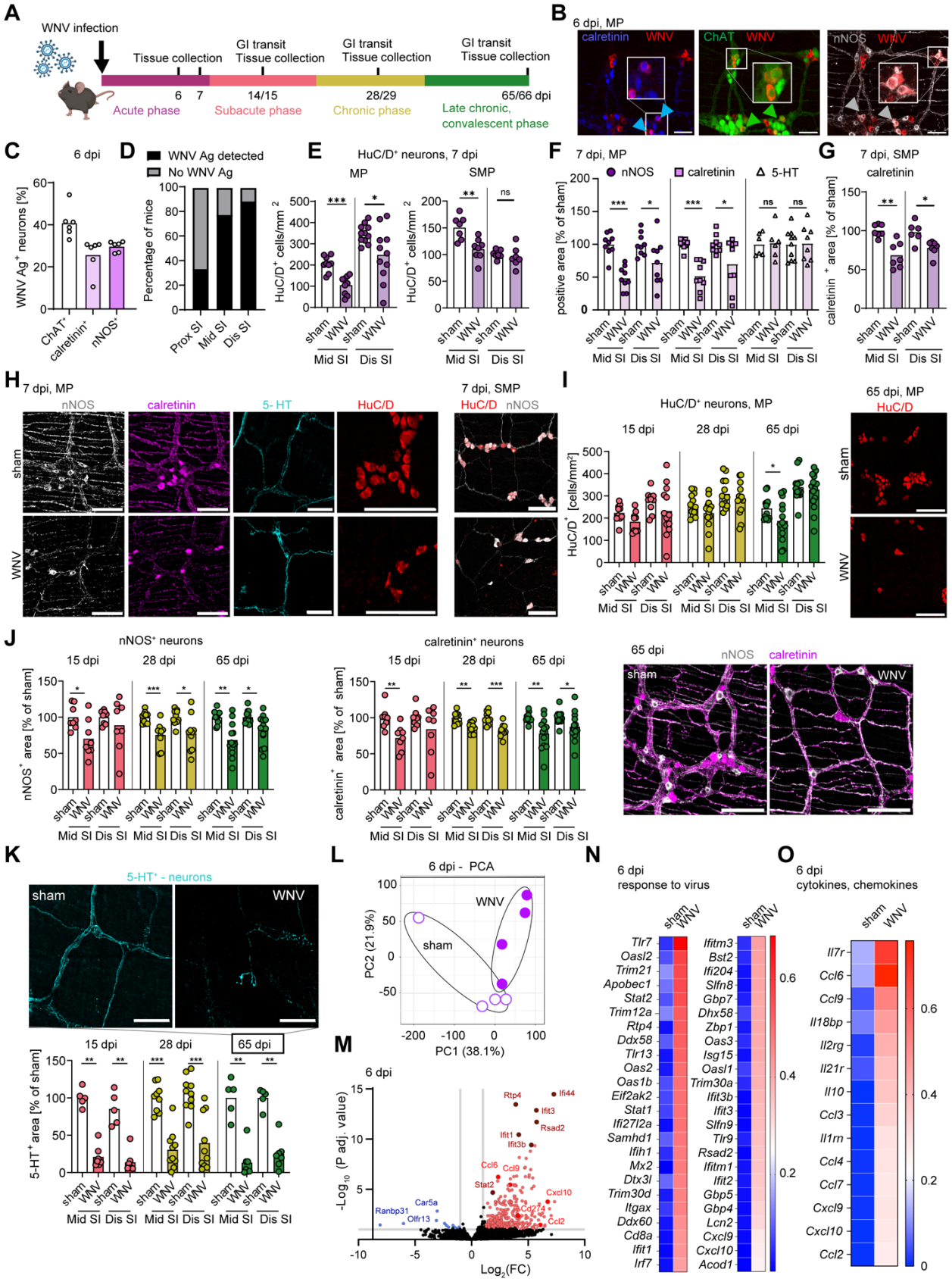
A
WNV infection
Tissue collection
GI transit Tissue collection
GI transit Tissue collection
GI transit Tissue collection
6
7
14/15
28/29
65/66 dpi
Acute phase
Subacute phase
Chronic phase
Late chronic, convalescent phase
B
6 dpi, MP
calretinin WNV
ChAT WNV
nNOS WNV
C
6 dpi
WNV Ag+ neurons [%]
ChAT+
calretinin+
nNOS+
D
WNV Ag detected
No WNV Ag
Percentage of mice
Prox SI
Mid SI
Dis SI
E
HuC/D+ neurons, 7 dpi
MP
SMP
HuC/D+ cells/mm 2
sham
WNV
Mid SI
Dis SI
ns
F
7 dpi, MP
nNOS
calretinin
5-HT
positive area [% of sham]
G
7 dpi, SMP
calretinin
calretinin+ area [% of sham]
H
7 dpi, MP
nNOS
calretinin
5- HT
HuC/D
7 dpi, SMP
HuC/D nNOS
sham
WNV
I
HuC/D+ neurons, MP
15 dpi
28 dpi
65 dpi
HuC/D+ [cells/mm2]
65 dpi, MP
HuC/D
J
nNOS+ neurons
calretinin+ neurons
15 dpi
28 dpi
65 dpi
nNOS+ area [% of sham]
calretinin+ area [% of sham]
65 dpi
nNOS
calretinin
sham
WNV
K
5-HT+ - neurons
sham
WNV
15 dpi
28 dpi
65 dpi
5-HT+ area [% of sham]
L
6 dpi - PCA
WNV
sham
PC2 (21.9%)
PC1 (38.1%)
M
6 dpi
-Log10 (P adj. value)
Log2(FC)
Rtp4
Ifi44
Ifit3
Rsad2
Ifit1
Ifit3b
Ccl6
Ccl9
Stat2
Cxcl10
Cd274
Ccl2
Ranbp31
Car5a
Olfr13
N
6 dpi
response to virus
Tlr7
Oasl2
Trim21
Apobec1
Stat2
Trim12a
Rtp4
Ddx58
Tlr13
Oas2
Oas1b
Eif2ak2
Stat1
Ifi27l2a
Samhd1
Ifih1
Mx2
Dtx3l
Trim30d
Itgax
Ddx60
Cd8a
Ifit1
Irf7
Ifitm3
Bst2
Ifi204
Slfn8
Gbp7
Dhx58
Zbp1
Oas3
Isg15
Oasl1
Trim30a
Ifit3b
Ifit3
Slfn9
Tlr9
Rsad2
Ifitm1
Ifit2
Gbp5
Gbp4
Lcn2
Cxcl9
Cxcl10
Acod1
O
6 dpi
cytokines, chemokines
Il7r
Ccl6
Ccl9
Il18bp
Il2rg
Il21r
Il10
Ccl3
Il1rn
Ccl4
Ccl7
Cxcl9
Cxcl10
Ccl2

Figure 1. WNV infection induces changes in ENS neuronal networks. (**A**) Timeline of WNV infection. 9 to 10-week-old C57BL6/J male mice were inoculated in the footpad with 10^2 FFU of WNV (New York 1999 strain), and carmine dye transit assay and tissue collections were performed at indicated time points. (**B-C**) Whole mount preparations of the muscularis externa from *ChAT*-eGFP reporter mice were isolated at 5 or 6 dpi and co-stained for WNV antigen, calretinin$^+$ and nNOS$^+$ neurons. (**B**) Blue, green, and white arrows indicate WNV antigen$^+$ calretinin$^+$ neurons, ChAT$^+$ neurons, and nNOS$^+$ neurons, respectively. Images are representative of 2 experiments; scale bar, 50 μm. (**C**) The proportion of specific neuronal subgroups infected with WNV. (**D**) Percentage of mice having WNV antigen in the proximal, middle (mid), and distal regions of small intestine (SI) at 6 dpi. (**E-K**) Muscularis externa with the attached layer containing submucosal plexus (SMP) (**G**), myenteric plexus (MP) (**F, I-K**), or with MP only or both MP and SMP, as indicated (**E**, **H**) was isolated from the mid and distal SI of sham or WNV-infected mice at 7 dpi (**E-H**) or 15, 28, and 65 dpi (**I-K**) and stained for neuronal markers. (**E, I**) The total number of HuC/D$^+$ neurons in (**E**) submucosal (SMP) and myenteric plexus (MP) or (**I**) MP only was counted and is shown as number of neurons per mm^2. (**F-G**) The fraction of area staining positive for nNOS, calretinin, and 5-HT in the MP (**F**) or calretinin in the SMP (**G**) was determined, and the values were normalized to sham-infected mice. Circles, squares, and triangles indicate nNOS$^+$, calretinin$^+$, and 5-HT$^+$ neurons, respectively. (**H**) Representative images show staining for indicated markers in mid SI in sham and WNV-infected mice at 7 dpi in either MP or SMP as indicated. Scale bar, 100 μm. (**J**) nNOS$^+$ and calretinin$^+$, and (**K**) 5-HT$^+$ cell area was determined, and the values were normalized to sham-infected mice. (**I-K**) Representative images show staining in mid SI in sham and WNV-infected mice at 65 dpi. Scale bar, 100 μm. (**L-O**) Analysis of neuron-specific RNA sequencing using TRAP in WNV or mock-infected *Snap25l10a* mice 6 dpi. (**L**) Principal component analysis (PCA). (**M**) Volcano plot of differential expression analysis (DEseq2) of Translating Ribosome Affinity Purification (TRAP)-seq comparing WNV and mock-infected samples. Red dots indicate $\log_2$ fold-change > 1, and FDR (p adjusted) < 0.05 while blue dots indicate $\log_2$ fold-change < -1 and p adjusted < 0.05. (**N-O**) Heatmap of differentially expressed genes in sham and WNV-infected mice showing genes related to (**N**) response to virus, and (**O**) cytokines and chemokines. Expression levels are normalized across each gene and represent the average of 4 mice per condition. Data are pooled from the following number of experiments: (**C-D**) 2; (**E-K**) 3 (MP) or 2 (SMP); (**F**) 3; (**G**) 2, (**I**) 3; (**J**) 2 (15 dpi), 3 (28 dpi), or 4 (65 dpi); (**K**) 2 (15 dpi), 3 (28 dpi), or 2 (65 dpi). The indicated numbers of mice per group were used (left to right): (**C**) 6, 6, 6; (**D**) 9, 9, 9; (**E**) 9, 9, 11, 11, 7, 8, 7, 7; (**F**) 9, 9, 9, 9, 9, 9, 9, 9, 6, 6, 10, 8; (**G**) 7, 7, 6, 7; (**I**) 10, 9, 10, 13, 13, 13, 13, 13, 13, 14, 16, 14, 16; (**J**) 8, 8, 8, 8, 10, 9, 10, 10, 12, 13, 12, 13, 8, 8, 8, 8, 10, 10, 10, 9, 12, 13, 12, 13; (**K**) 5, 7, 5, 7, 9, 10, 10, 10, 5, 7, 5, 7. (**C, E-G, I-K**) Column heights indicate mean values. Statistical analysis: two-tailed Mann-Whitney test: not significant, ns, *p < 0.05, **p < 0.01, ***p < 0.001.

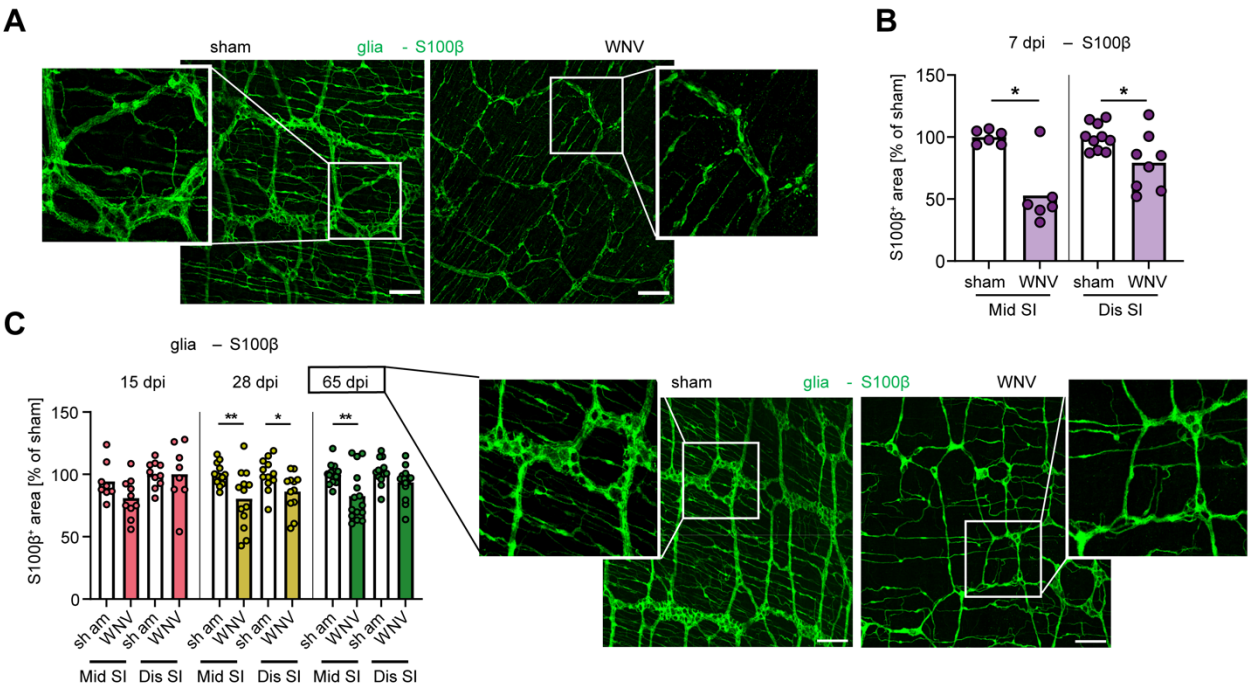

Figure 2. WNV infection affects enteric glial networks. (**A-C**) Muscularis externa was isolated from mid and distal regions of small intestine (SI) of sham or WNV-infected C57BL/6J mice at (**A-B**) 7 dpi or (**C**) 15, 28, and 65 dpi and stained for glia (S100β). The fraction of area staining positive for S100β was determined, and the values were normalized to sham-infected mice. Representative images show S100β staining in the mid region of SI in sham and WNV-infected mice at 7 (**A**) or 65 (**C**) dpi; scale bar, 100 μm Data are pooled from (**A**, **B**) 2 experiments, n = 5-10 per group; (**C**) from left to right: 2, 3, 4 experiments, n = 6-10, 12-13, 13-16. Column heights indicate mean values. Statistical analysis: two-tailed Mann-Whitney test: not significant, ns, *p < 0.05, **p < 0.01, ***p < 0.001.

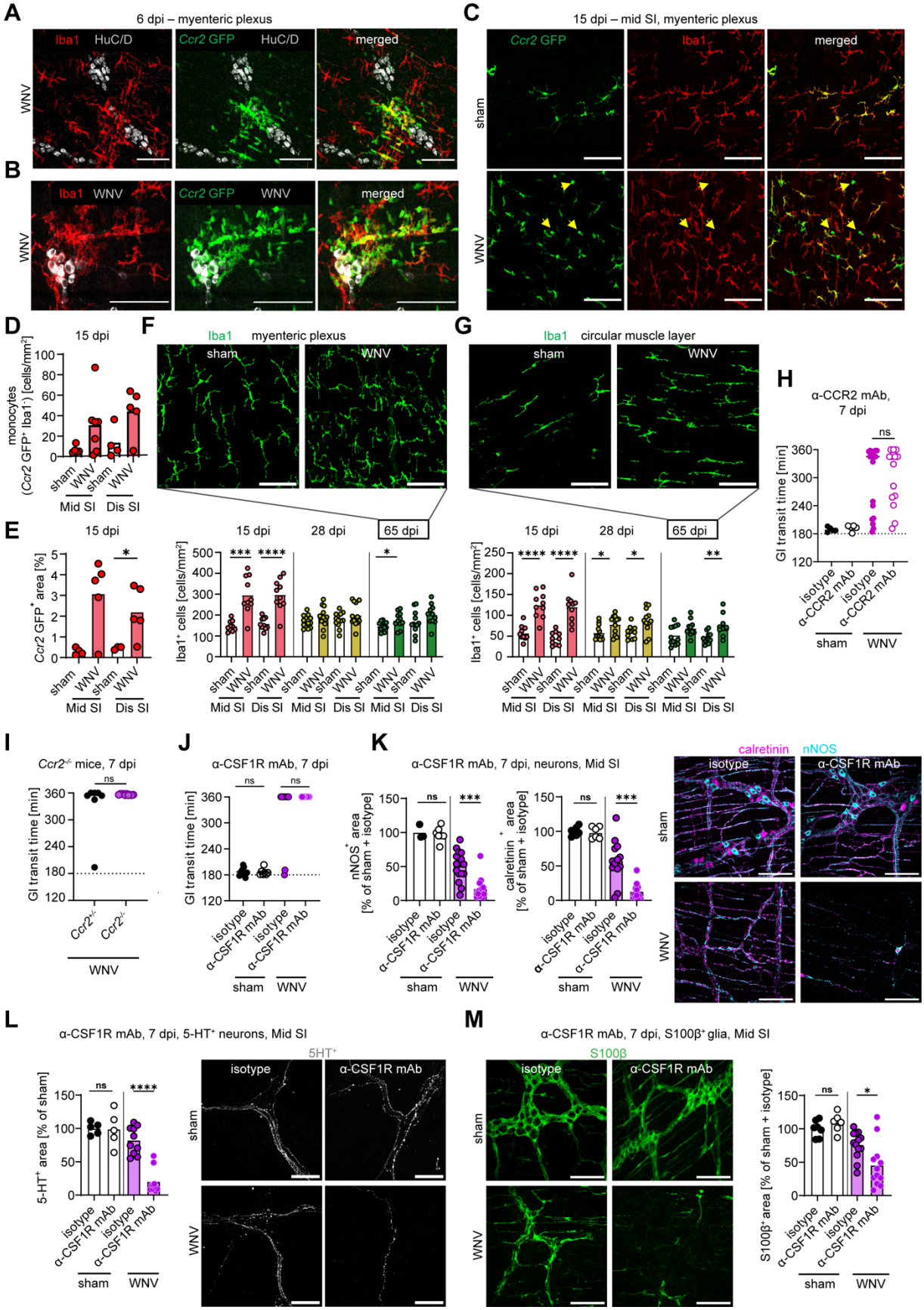
A
6 dpi – myenteric plexus
Iba1 HuC/D
Ccr2 GFP HuC/D
merged
WNV
B
Iba1 WNV
Ccr2 GFP WNV
merged
WNV
C
15 dpi – mid SI, myenteric plexus
Ccr2 GFP
Iba1
merged
sham
WNV
D
15 dpi
monocytes (Ccr2 GFP+ Iba1-) [cells/mm2]
sham WNV sham WNV
Mid SI Dis SI
E
15 dpi
Ccr2 GFP+ area [%]
*
sham WNV sham WNV
Mid SI Dis SI
15 dpi 28 dpi 65 dpi
Iba1+ cells [cells/mm2]
*** **** *
Mid SI Dis SI Mid SI Dis SI Mid SI Dis SI
F
Iba1 myenteric plexus
sham
WNV
G
Iba1 circular muscle layer
sham
WNV
15 dpi 28 dpi 65 dpi
Iba1+ cells [cells/mm2]
**** **** * * **
Mid SI Dis SI Mid SI Dis SI Mid SI Dis SI
H
α-CCR2 mAb, 7 dpi
GI transit time [min]
ns
isotype α-CCR2 mAb isotype α-CCR2 mAb
sham WNV
I
Ccr2-/- mice, 7 dpi
GI transit time [min]
ns
Ccr2+/- Ccr2-/-
WNV
J
α-CSF1R mAb, 7 dpi
GI transit time [min]
ns ns
isotype α-CSF1R mAb isotype α-CSF1R mAb
sham WNV
K
α-CSF1R mAb, 7 dpi, neurons, Mid SI
nNOS+ area [% of sham + isotype]
ns ***
calretinin+ area [% of sham + isotype]
ns ***
isotype α-CSF1R mAb isotype α-CSF1R mAb
sham WNV
calretinin nNOS
isotype
α-CSF1R mAb
sham
WNV
L
α-CSF1R mAb, 7 dpi, 5-HT+ neurons, Mid SI
5-HT+ area [% of sham]
ns ****
isotype α-CSF1R mAb isotype α-CSF1R mAb
sham WNV
5HT+
isotype
α-CSF1R mAb
sham
WNV
M
α-CSF1R mAb, 7 dpi, S100β+ glia, Mid SI
S100β
isotype
α-CSF1R mAb
sham
WNV
S100β+ area [% of sham + isotype]
ns *
isotype α-CSF1R mAb isotype α-CSF1R mAb
sham WNV

943

Figure 3. WNV infection promotes infiltration of monocytes into the intestine. (**A-E**) Whole mount preparations of the muscularis externa were isolated from the middle and distal regions of small intestine (SI) of WNV-infected heterozygous *Ccr2*-GFP mice at (**A, B**) 6 or (**C**) 15 dpi and stained for (**A**) neuron (HuC/D) and macrophage (Iba1) markers, (**B**) WNV antigen and macrophage markers, or (**C-E**) macrophage markers. Yellow arrows indicate monocytes (CCR2 GFP^+ $Iba1^-$ cells). Scale bar, 100 μm. (**A-C**) Representative images are obtained from the myenteric plexus of the mid region of SI from at least 2 experiments. (**D**) Monocytes (*Ccr2* GFP^+ $Iba1^-$) in the myenteric plexus are shown as the numbers of cells per mm^2. (**E**) The fraction of *Ccr2* GFP-positive area (representing monocytes and/or monocyte-derived macrophages) in the myenteric plexus of WNV- or sham-infected mice. (**F-G**) Muscularis externa of mid and distal SI from sham or WNV-infected mice harvested at 15, 28, or 65 dpi were stained for macrophages (Iba1). Macrophages in (**F**) the myenteric plexus and (**G**) the circular muscle layer are shown as the number of $Iba1^+$ cells per mm^2. Images are representative of Iba1 staining in sham or WNV-infected mice at 65 dpi. Scale bar, 100 μm. (**H-J**) GI transit was measured after oral gavage of carmine red dye (**H**) in sham or WNV-infected mice (at 7 dpi) after treatment with anti-CCR2 or isotype mAbs, (**I**) in WNV-infected $Ccr2^{+/-}$ and $Ccr2^{-/-}$ mice, (**J**) in sham or WNV-infected mice after treatment with anti-CSF1R or isotype control mAb. (**K-M**). Whole mount preparations of the muscularis externa were isolated from the middle region of SI of WNV-infected mice treated with anti-CSF1R or isotype mAbs and stained for (**K**) $nNOS^+$ and $calretinin^+$ neurons, (**L**) 5-HT^+ neurons or (**M**) $S100\beta^+$ glia. Scale bar, 100 μm. The fraction of area staining positive for calretinin, nNOS, 5-HT or S100β was determined, and values were normalized to sham-infected mice treated with isotype control mAb. Data are pooled from: (**D, E**) 2, (**F, G**) 2 (15 dpi), 3 (28 dpi), 4 (65 dpi); (**H**) 3; (**I**) 1; (**J**) 3; (**K-M**) 3 experiments with indicated numbers of mice per group (from left to right): (**D, E**) 4, 7, 4, 7; (**F**) 9, 10, 10, 10, 13, 13, 13, 11, 11, 12, 11; (**G**) 10, 10, 10, 10, 12, 12, 11, 12, 12, 11, 11, 11; (**H**) 5, 5, 20, 15; (**I**) 7,10; (**J**) 9, 7, 16, 15; (**K**) 7, 6, 13, 12; (**L**) 5, 5, 10,10; and (**M**) 7, 7, 13, 12. (**D-G** and **J-L**). Column height indicates mean values. (**H-J**) Lines indicate median values. Statistical analysis: (**D, F-G**) Two-tailed Mann-Whitney test; (**L**) Kruskal-Wallis ANOVA with Dunn's post-test. Not significant, ns, *$p < 0.05$, **$p < 0.01$, ***$p < 0.001$, ****$p < 0.0001$.

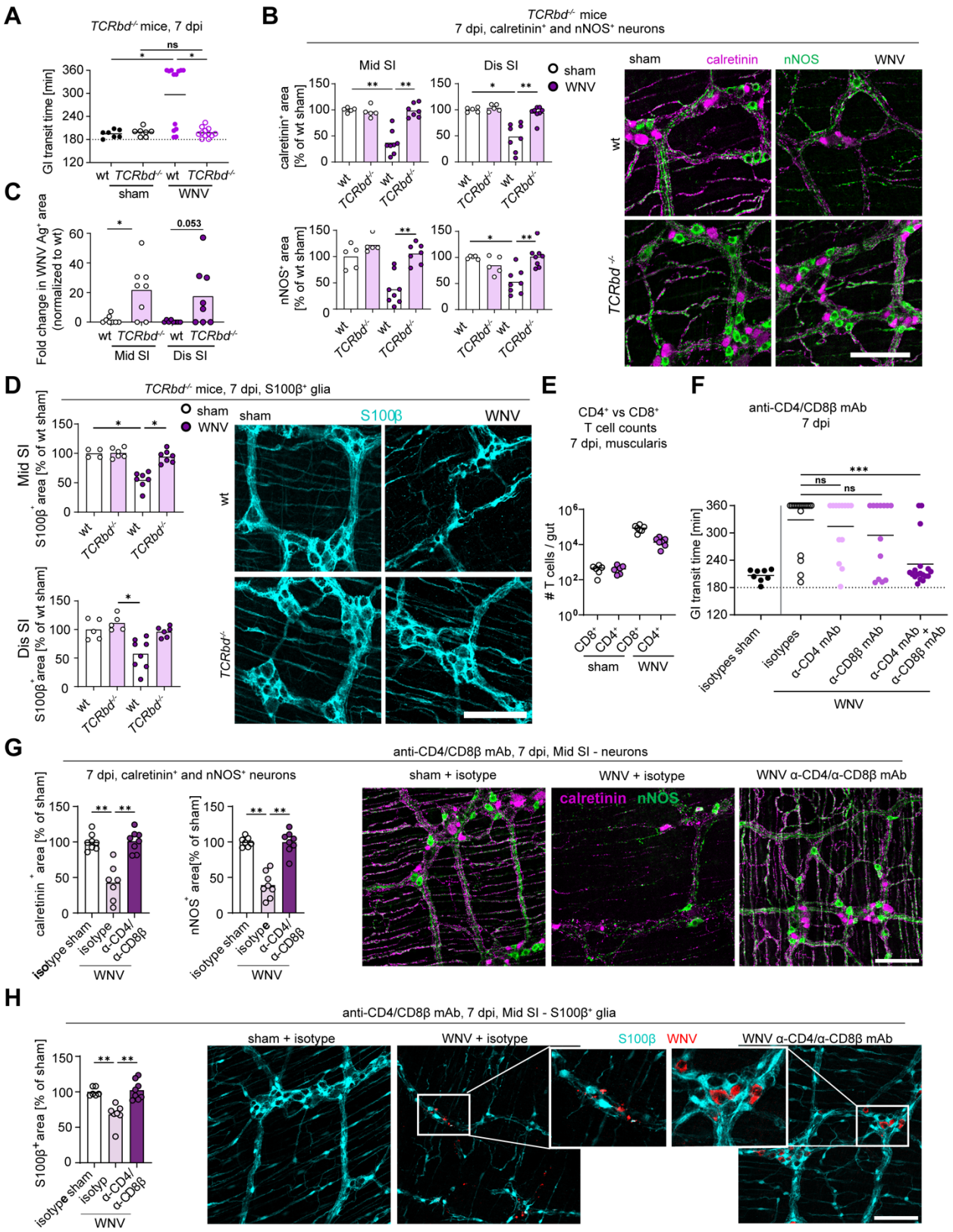

Figure 4. Damage to neuronal and glial network is caused by CD4$^+$ and CD8$^+$ T cells. (**A, F**) GI transit was measured after oral gavage of carmine red dye. (**A**) Transit time in sham or WNV-

infected wt or *TCRbd*$^{-/-}$ mice at 7 dpi. (**B, C, D, G, H**). Muscularis externa was isolated from (**B, C, D**) middle and distal regions of small intestine (SI) of sham or WNV-infected wt or *TCRbd*$^{-/-}$ mice at 7 dpi, (**G, H**) middle regions of SI sham or WNV-infected wt mice at 7 dpi treated with anti-CD4 and/or anti-CD8β or isotype control mAbs and stained for (**B, G**) calretinin^{+} and nNOS^{+} neurons, (**C**) WNV antigen, (**D**) S100β^{+} glia, or (**H**) and S100β^{+} glia and WNV antigen. The fraction of area staining positive for calretinin, nNOS or S100β was determined, and the values were normalized to (**B, D**) wt sham-infected mice or (**G-H**) animals treated with isotype control mAb. Representative images from the myenteric plexus of the middle region of SI, scale bar, 100 μm. (**C**) Data are presented as the percentage of WNV antigen-positive area in the field of view. (**E**) Counts of live CD45^{+} TCRβ^{+} CD4^{+} or CD8^{+} T cells in muscularis of sham or WNV-infected C57BL6/J mice at 7 dpi. (**F**) Transit time of sham or WNV-infected mice at 7 dpi treated with anti-CD4 and/or anti-CD8β or isotype control mAbs. Data are pooled from (**A**) 3; (**C-E, G**) 2; and (**F**) 4 experiments with indicated numbers of mice per group (left to right): (**A**) 7, 7, 13, 12; (**C-D**) 5, 5, 8, 7; (**E**) 6, 6, 7, 7; (**F**) 8, 18, 10, 10, 18; (**G)** 8, 7, 8, 7, 8, 8; (**H**) 6, 7, 8. (**A, E, F**) Lines indicate the mean values. (**B, C, D, G, H**) Column height indicates mean values. Statistical analysis: (**A**, **B, D, G, H**) Kruskal-Wallis ANOVA with Dunn's post-test (all groups compared to each other); (**F**) Kruskal-Wallis ANOVA with Dunn's post-test (comparison to "isotype control" group); and (**C**) two-tailed Mann-Whitney test: not significant, ns, *$p < 0.05$, **$p < 0.01$, ***$p < 0.001$.

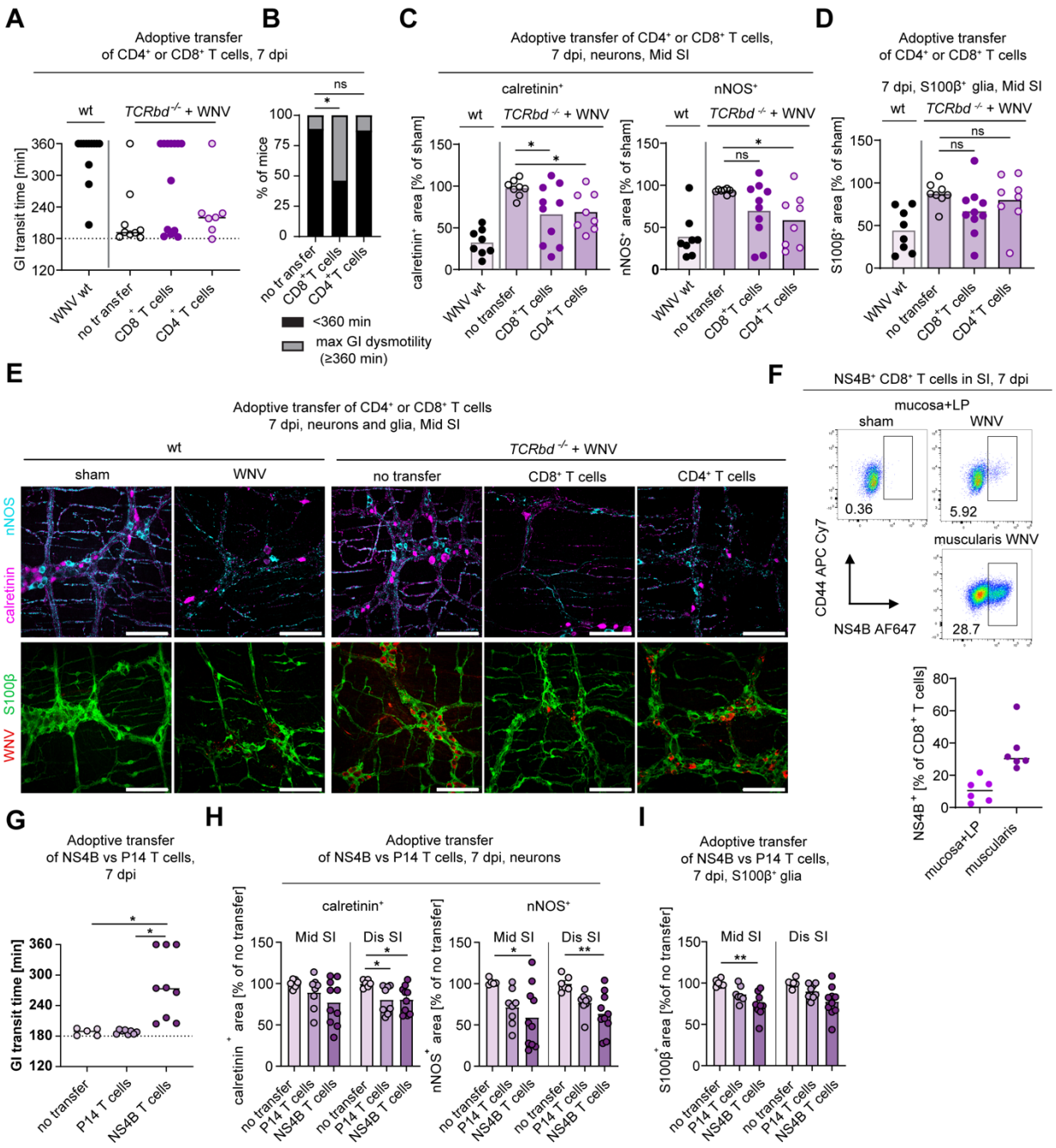

Figure 5. Damage to neuronal and glial network is caused by WNV-specific CD8$^+$ and CD4$^+$ T cells. (**A-E**) Adoptive transfer of WNV-primed wt CD4$^+$ or CD8$^+$ T cells to *TCRbd*$^{-/-}$ mice. CD4$^+$ or CD8$^+$ T cells from WNV-infected wt mice were isolated at 7 dpi and adoptively transferred to *TCRbd*$^{-/-}$ at 2 dpi. (**A**) GI transit time in recipient *TCRbd*$^{-/-}$ mice at 7 dpi, (**B**) proportions of mice with severe GI dysmotility (≥ 360 min), (**C-D**) analysis of neuronal (calretinin, nNOS) and glial (S100β) networks from middle small intestine (SI) at 7 dpi, and (**E**) representative images obtained from the myenteric plexus of the middle region of SI, scale bar, 100 µm. (**F**) Flow cytometric analysis of muscularis externa or mucosa and lamina propria at 7 dpi. Cells were stained with

mAbs to CD45, TCRβ, TCRγδ, CD8a, CD44, and WNV NS4B D^b-restricted tetramers and gated on live $CD45^+$ $TCR\beta^+$ $CD8^+$ cells (see **Fig S4C**). Graph shows percentage of $CD8^+$T cells positive for NS4B. (**G-I**) Adoptive transfer of $CD8^+$ T cells from P14 transgenic mice (targeting LCMV gp33 peptide) or WNV NS4B transgenic mice to *TCRbd*$^{-/-}$ mice. T cells were administered to *TCRbd*$^{-/-}$ mice one day prior to subcutaneous inoculation with WNV. (**G**) GI transit 7 dpi, (**H-I**) analysis of neuronal (calretinin, nNOS) and glial network (S100β) from mid and distal SI at 7 dpi. (**A, G**) GI transit was measured after oral gavage of carmine red dye. (**C, D, H, I**) The fraction of area positive for calretinin, nNOS or S100β was determined, and values were normalized to (**C, D**) wt sham mice or (**H, I**) *TCRbd*$^{-/-}$ mice without adoptive transfer. Data are pooled from, (**A, B, C, D**) 6; (**F**) 2; and (**G-I**) 3 experiments with indicated numbers of mice per group (left to right): (**F**) 6; (**A**) 13, 12, 9, 13, 8; (**B**) 9, 13, 8; (**C, D**) 11, 9, 13, 8; (**F**) 6, 6; (**G**) 5, 8, 9; (**H, I**) 6, 8, 10, 6, 8, 10. Lines indicate (**G, F**) median and column heights indicate (**C, D, H, I**) mean values. Statistical analysis: (**C, D**) ANOVA with Dunnett's post-test (comparison to "no transfer" group); (**B**) Chi-squared test with Bonferroni correction (proportions compared to "no transfer" group); and (**G-I**) Kruskal-Wallis ANOVA with Dunn's post-test (comparison to "no transfer" group): not significant, ns, *$p < 0.05$, **$p < 0.01$.

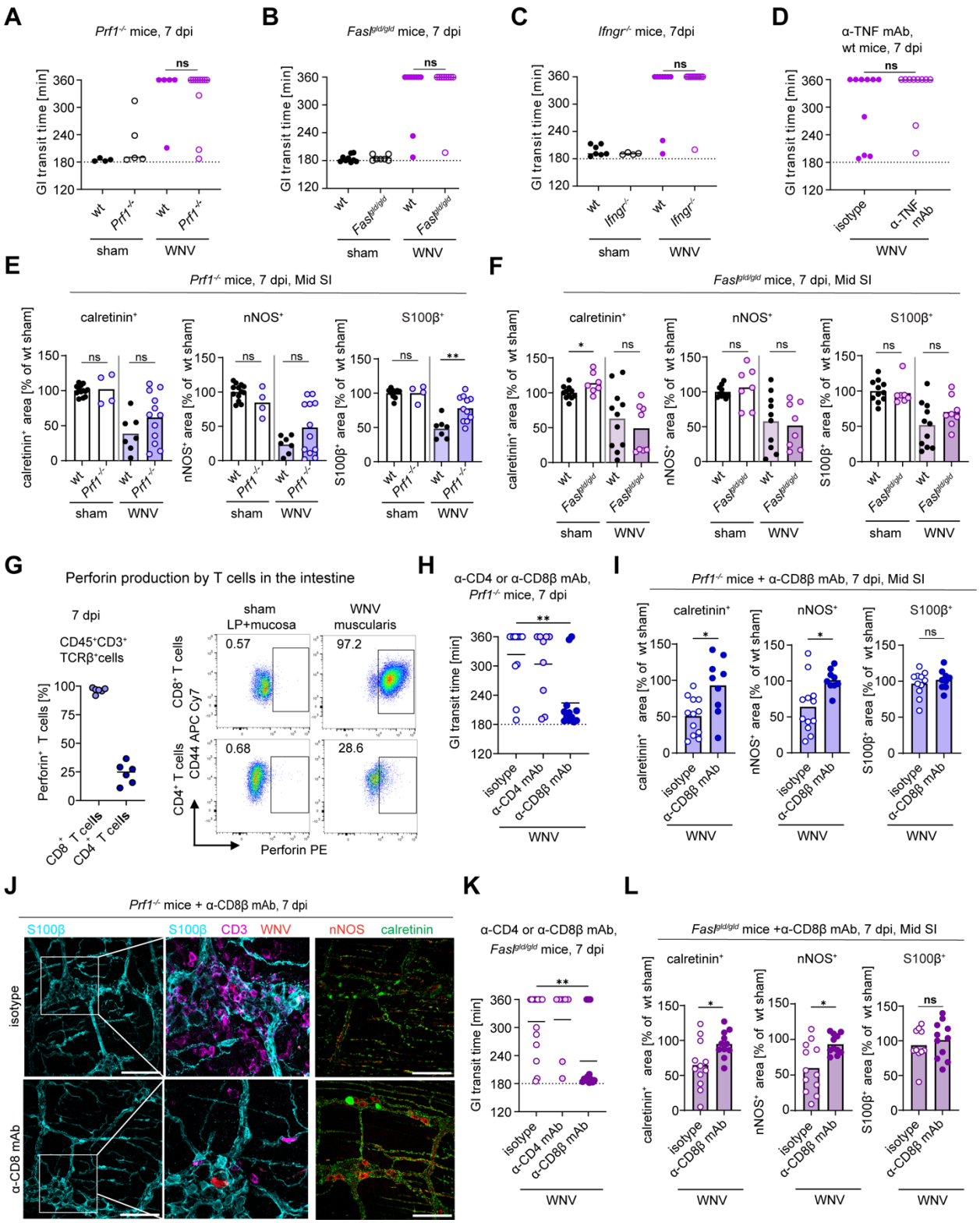

Figure 6. CD4⁺ and CD8⁺ T cells injure neurons and glia using multiple effector functions. (**A, B, C, D, H, K**) GI tract transit was measured after oral gavage of carmine red dye at 7 dpi. Transit time of sham, WNV-infected wild-type (*WT*) or WNV-infected (**A**) *Prf1*$^{-/-}$ mice, (**B**) *Fasl*$^{gld/gld}$

mice, (**C**) *Ifngr*$^{-/-}$ mice, (**D**) wt mice treated with anti-TNF or isotype control mAb or WNV-infected, (**H**) *Prf1*$^{-/-}$ mice or (**K**) *Fasl*$^{gld/gld}$ mice treated with anti-CD4, anti-CD8β or isotype control mAb. (**E, F, I, J, L**) Muscularis externa was isolated from mid regions of small intestine (SI) of sham, WNV-infected wt or *Prf1*$^{-/-}$ (**E**), *Fasl*$^{gld/gld}$ (**F**) or WNV-infected *Prf1*$^{-/-}$ (**I, J**) or *Fasl*$^{gld/gld}$ (**L**) mice treated with anti-CD4 or anti-CD8β mAb at 7 dpi and stained. The fraction of positive area for calretinin, nNOS or S100β was determined, and values were normalized to sham-infected wt mice. (**J**) Representative images are obtained from the myenteric plexus of the middle region of the SI, scale bar 100 μm. Data are pooled from: (**A, B, C, F, I, J**) 3; (**D, G, L**) 2; (**E, K**) 5; and (**H**) 4 experiments with indicated numbers of mice per group (left to right): (**A**) 4, 4, 5, 11; (**B**) 9, 7, 10, 9; (**C**) 7, 4, 9, 11; (**D**) 10, 10; (**E**) 13, 4, 7, 12, 13, 4, 7, 12, 10, 4, 7, 11; (**F**) 11, 7, 11, 8, 10, 7, 10, 8, 11, 7, 11, 8 6; (**G**) 6, 6; (**H**) 12, 9, 12; (**I**) 12, 9, 12, 9, 11, 9; (**K**) 15, 7, 13; (**L**) 7, 6, 7, 6, 7, 6. Lines indicate (**A-D, G**) median or (**H, K**) mean. Column heights indicate mean values. Statistical analysis: (**A-F, I, L**) Mann-Whitney test; (**H, K**) ANOVA with Dunnett's post-test (comparison to "isotype control" group): not significant, ns, *$p < 0.05$, **$p < 0.01$.

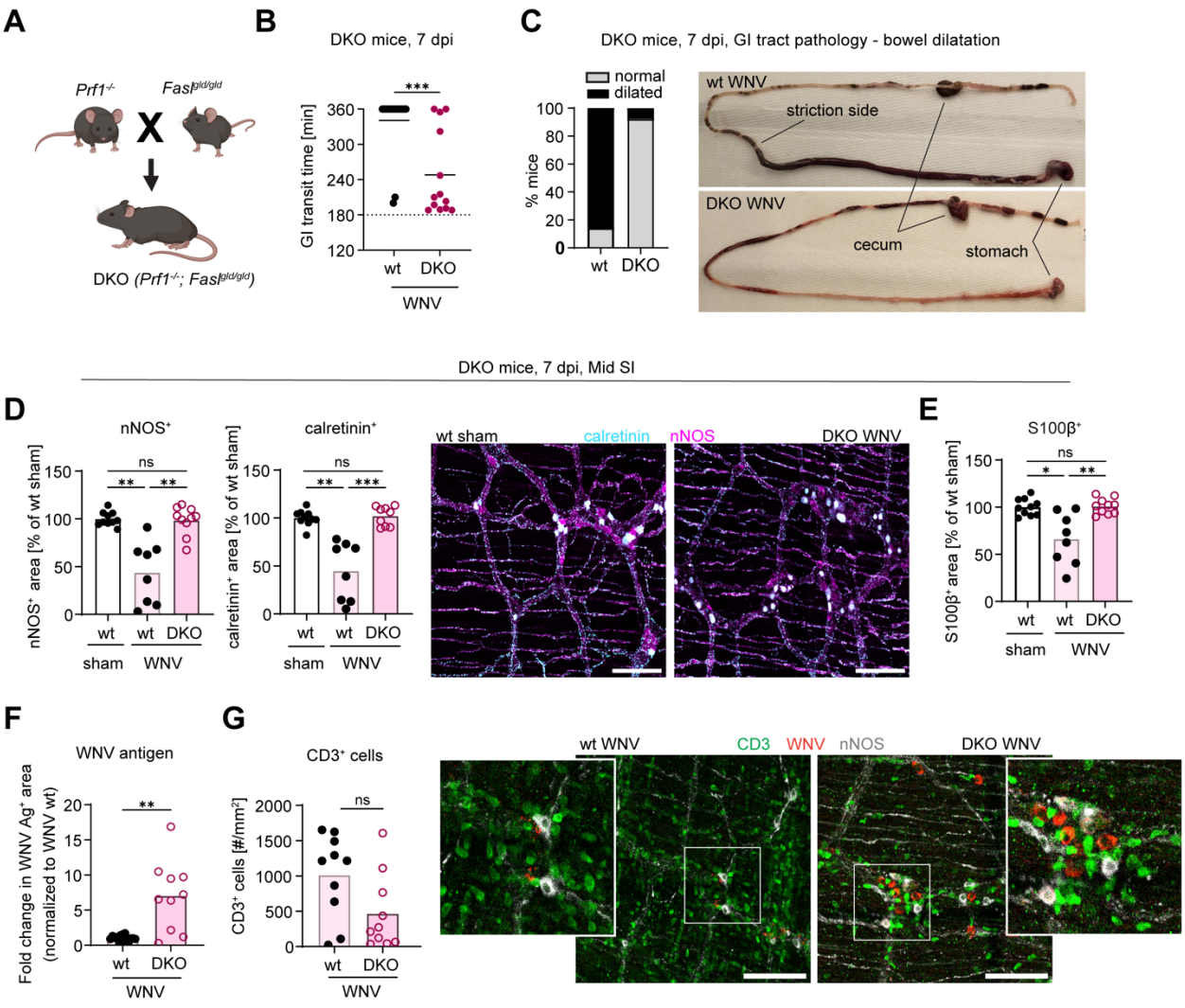

Figure 7. Mice lacking perforin and Fas-FasL signaling do not develop WNV-triggered GI dysmotility or neuronal and glial network injury. (**A**) Scheme of generation of *Prf1*$^{-/-}$*; Fasl*$^{gld/gld}$ (DKO) mice. (**B**) GI transit time in WNV-infected wt or DKO mice at 7 dpi. (**C**) Proportions of WNV-infected wt and DKO mice showing abnormal bowel dilation in the small intestine (SI) at 7 dpi. (**D-G**) Muscularis externa was isolated from middle regions of SI of sham (**D, E**) or WNV-infected wt or DKO (**F, G**) mice at 7 dpi and stained. (**D-F**) The fraction of positive area for calretinin, nNOS, S100β, and WNV antigen was determined, and values were normalized to (**D, E**) sham-infected wt mice or (**F**) to WNV-infected wt mice. (**G**) Numbers of CD3$^+$ cells in the myenteric plexus were calculated by dividing the area positive for CD3$^+$ staining with average size of CD3$^+$ cell. Cell counts are expressed as numbers of CD3$^+$ cells per mm^2. (**D, G**) Representative images are obtained from the myenteric plexus of the middle region of small intestine, scale bar 100 µm. Data are pooled from: (**B, C, F**) 5 and (**D, E, G**) 4 experiments with indicated numbers of mice per group (left to right): (**B, C**) 16, 13; (**D, E**) 10, 8, 10; (**F**) 15, 10; and (**G**) 10, 10. (**B**) Lines and (**D-G**) column heights indicate mean values. Statistical analysis: (**B, F, G**) Two-tailed Mann-Whitney test; (**D, E**) Kruskal-Wallis ANOVA with Dunn's post-test. Not significant, ns, *p < 0.05, **p < 0.01, ***p < 0.001.

Supplemental Material

West Nile virus triggers intestinal dysmotility via T cell-mediated enteric nervous system injury

Hana Janova[1], Fang R. Zhao[1], Pritesh Desai[1], Matthias Mack[2], Larissa B. Thackray[1], Thaddeus S. Stappenbeck[3]*, and Michael S. Diamond[1,4,5,6]*

Materials and Methods

Immunofluorescence microscopy. Intestines were harvested from isoflurane overdosed mice at indicated time points after WNV inoculation. To examine the middle region of the small intestine, 5 cm from the same anatomical regions were used. Distal small intestine regions were defined as last 5 cm preceding the cecum, and the proximal part of small intestine was defined as the first 2 cm of small intestine. The intestinal contents were flushed out sequentially with PBS and 4% paraformaldehyde (PFA). The tissue was opened along the mesenteric border, uniformly stretched, pinned to Sylgard silicon plates, and fixed in 4% PFA overnight at 4°C. The fixed tissue was washed three time in PBS and unless processed at the same day, stored in 0.02% NaN_3 in PBS. For whole mount staining of myenteric plexus, the mucosa and muscularis mucosa together with the attached submucosal plexus were dissected away from the muscularis externa. To analyze the submucosal plexus, the mucosa was scratched and muscularis mucosae was carefully dissected leaving the submucosal layer intact. All dissections were performed using a dissecting microscope (Olympus SZX7). The dissected tissue was blocked for at least 1 h at room temperature (RT) in blocking buffer (5% normal donkey serum (NDS) + 1% bovine serum albumin (BSA) + 1% Triton X-100 in 1x PBS or 1x Tris buffered saline (TBS) (WNV antigen staining) and incubated overnight in 3% NDS + 1% BSA + 1% Triton X-100 in 1x PBS with primary antibodies

against nNOS (goat, 1:500, Abcam; # Ab1376), nNOS (goat, 1:500, Millipore; # AF2416), calretinin clone DC8 (rabbit, 1:500, ThermoFisher Scientific, # 180211), Iba1 (rabbit, 1:500, Abcam; # ab178846), HuC/D (biotinylated mouse, 1:150, ThermoFisher Scientific, # A21272), Tuj1 (rabbit, 1:500, Abcam, # ab18207), serotonin (goat, 1:500, Immunostar, # 20079), S100β clone EP1576Y (rabbit, 1:500, 1:500, Abcam, , # ab52642), cKit (goat, 1:200, R&D, # AF1356), CD3 (rabbit, 1:150, Abcam, # ab5690), CD3 (Armenian hamster, 1:100, eBioscience, # 13-0031-8), CD4 (rat, 1:150, eBioscience, # 14-0041-82), CD8b APC (rat, 1:150, BioLegend, # 126613), peripherin (rabbit, 1:1,000, Millipore, # AB1530), or in 3% NDS + 1% BSA + 1% Triton X-100 in TBS with rat anti-WNV polyclonal serum (1:500) (1) at 4°C. For HuC/D staining, tissue was pre-treated with Avidin/Biotin Blocking Kit (Vector Laboratories; # SP-2001) following the manufacturer instructions. Tissue was washed three times with PBS + 1% Triton X-100 and incubated for 1 h at room temperature with secondary antibodies: donkey anti-rabbit Alexa Fluor 488, 647, 546 (1:500, ThermoFisher Scientific, # A31573, A21206, A10040) or DyLight 405 (1:250, Jackson ImmunoResearch laboratories, # 711-475-152), donkey anti-goat Alexa Fluor 488, 647, 546 (1:500, ThermoFisher Scientific, # A11055, A32849, A11056) and donkey anti-rat Alexa Fluor 555, 488, 647 (1:500, ThermoFisher Scientific, # A78945, A21208, S78947) or Streptavidin Alexa Fluor 546 (1:500, ThermoFisher Scientific, # S11225) in PBS or TBS + 3% NDS + 1% BSA +1% Triton X-100. Subsequently, tissue sections were washed three times in PBS + 1% Triton X-100, counterstained for nuclei with Hoechst 33342 dye in PBS (1:5,000, ThermoFisher Scientific) and mounted in Aqua-Poly/Mount (Polysciences) or ProLong™ Glass Antifade Mountant (ThermoFisher Scientific, # P36980).

Images were captured on a Zeiss LSM880 Laser Scanning Confocal microscope using 20x (NA 0.8) or 40x (NA 1.4) objective. The scanned images were processed and analyzed by Fiji software (https://fiji.sc/Fiji). To quantify the density of neuronal (peripherin, nNOS, calretinin, 5-HT), glial (S100β) and ICCs (cKit) networks, four to five random regions (0.65 mm^2) were scanned using 20x (NA 0.8) objective and stitched (ZEN black software, Zeiss). To assess the level of WNV

infection, 4 mm^2 regions of tissue were scanned and stitched (ZEN black software, Zeiss). For all images, the background signal was uniformly subtracted (rolling ball, radius 50). Quantification was performed by converting images to binary using a threshold tool, and a fraction of total area was measured. For cell density analysis, the median value from each 4-5 images was calculated for every mouse and normalized to values of respective controls (as described in the legends).

The fraction of total area with WNV-antigen staining in *TCRbd*$^{-/-}$ *and DKO (Prf1*$^{-/-}$*; FasL*$^{gld/gld}$*)* mice was expressed as a fold change of value assessed in wt mice. To determine the cell numbers, five random regions (0.65 mm^2) were scanned using 20x (NA 0.8) objective and stitched (ZEN black software, Zeiss). The cells were counted manually by a blinded investigator using Cell counter Plugin of Fiji software. Values were expressed as numbers of cells per mm^2.

Translating ribosomal affinity purification (TRAP) and RNA-sequencing. Nine-to-ten week old hemizygous *Snap25l10a* GFP females (B6;FVB-Tg(Snap25-EGFP/Rpl10a)JD362Htz/J; JAX #:030273) were sacrificed with an overdose of isoflurane at 6 dpi. Five cm of distal small intestine was thoroughly flushed with RNAse-free PBS and put on a glass bar. After making a superficial dent with fine forceps, the muscularis externa was isolated. Samples were manually homogenized using a glass dounce tissue grinder (DWK Life Sciences; #8853000007) in homogenization buffer (50 mM Tris, pH 8.0; 100 mM KCl; 12 mM $MgCl_2$; 1 % Igepal; 1 mg/mL sodium heparin; 100 µg/mL cycloheximide; 0.2 U/µL SUPERaseIn RNase Inhibitor, 2 mM DTT). After centrifugation (10,000 x g; 10 min; 4^oC) 25 µg of primary antibody against GFP (rabbit; # AB290; Abcam) was added, and samples were rotated for 1 h at 4 ^oC. Subsequently, 200 µl of Dynabeads^{TM} Protein G (# 10004D; Invitrogen) were added, and samples were incubated rotating overnight at 4 C. The beads were washed four times with high-salt buffer (50 mM Tris, pH 8.0; 300 mM KCl; 12 mM $MgCl_2$; 1 % Igepal; 100 µg/mL cycloheximide). RNA was extracted and purified with Arcturus PicoPure RNA Isolation Kit (ThermoFisher: Kit0204 - Applied biosystems; 12204-01) according to the manufacturer's instructions. To prevent contamination with DNA, RNase-Free DNase Set (Qiagen; # 29254) was used according to the manufacturer's instructions.

RNA integrity was determined using Agilent Bioanalyzer or 4200 Tapestation. Library preparation was performed with 1-50 ng of total RNA. cDNA was prepared using the SeqPlex RNA Amplification Kit (Sigma) per manufacturer's protocol and then fragmented using a Covaris E220 sonicator using peak incident power 18, duty factor 20%, cycles per burst 50 for 120 seconds. cDNA was blunt ended, an A base was added to the 3' ends, and then Illumina sequencing adapters were ligated to the ends. Ligated fragments were then amplified for 12-15 cycles using primers incorporating unique index tags. Fragments were sequenced on an Illumina NovaSeq-6000 using paired end reads extending 150 bases.

Differential gene expression analysis. Sequencing data was demultiplexed using Illumina's DRAGEN and BCLconvert version 4.2.4 software. Reads were then aligned and mapped to the Ensembl release 101 primary assembly with STAR version 2.7.9a (2). A count matrix containing all expression data was then generated from the number of uniquely aligned unambiguous read using Subread:featureCount version 2.0.3 and isoform expression of known Ensembl transcripts quantified with Salmon version 1.5.2 (3, 4). Sequencing performance was assessed for the total number of aligned reads, total number of uniquely aligned reads, and features detected. Genes with low expression across all libraries were then filtered out and expression data was analyzed using DESeq2 with standard parameters, normalization, and the Benjamini-Hochberg adjustment to estimate the false discovery rate (FDR) and correct for multiple testing (5). Differentially expressed genes were ranked by absolute fold-change in gene expression (cutoff log2 fold change > 1) and filtered by significant FDR-corrected p-values (Padj < 0.05). Pathway analyses of differentially expressed genes were performed using the Gene Ontology (GO) databases (6, 7).

Flow cytometry. Blood was collected by submandibular bleeding, transferred to EDTA coated tubes (BD, # 365974), and erythrocytes were lysed by ACK lysis buffer (GIBCO) for 10 to 15 min at RT. After washing with FACS buffer (PBS supplemented with 2% FBS, 2 mM EDTA), Fc-gamma receptors were blocked (anti-CD16/32; Biolegend, # 101301), cells were stained with

viability dye (Zombie NIR; Biolegend, # 423105) and antibodies against CD45 BUV 395 (BD Bioscience, # 564279), CD11b PE (Biolegend, # 101208) , Ly6G PerCP (Biolegend, # 127616) Cy5.5, Ly6C BV421 (Biolegend, # 128031), and then fixed with 2% PFA. Samples were read on BD Fortessa X-20 and analyzed using FlowJo software (FlowJo LLC). For total cell counts, Trucount Absolute counting tubes were used (BD Biosciences, # 340334) according to the manufacturer's instructions.

Organs were harvested from isoflurane-overdosed mice. Single cell suspensions from spleens, Peyer's patches, and mesenteric lymph nodes were obtained by mashing through a cell strainer (70 μm) with syringe plunger, and erythrocytes in spleens were lysed by ACK lysis buffer (GIBCO) for 3 min on ice and then washed with FACS buffer. The small intestine was harvested, cut into 5 cm pieces, flushed with PBS and put on a glass bar. After making a superficial dent with fine forceps, the muscularis externa was isolated by rolling away with cotton Q-tip. The muscularis externa and the remainder of the gut were cut separately into small pieces (0.5 mm) and incubated with digestion buffer (RPMI 1640 Medium, 10% FBS, 1 mM sodium pyruvate, 1 mM HEPES, MEM Nonessential amino acids, β-mercaptoethanol or HBSS with Mg^{2+}/Ca^{2+} (Gibco, # 24020117), 400 U/mL collagenase D, 2.5 U/mL dispase, 25 mM HEPES, 1 mM sodium pyruvate, 50 μg/mL DNase I) at 37°C on shaker (140 rpm) for 40 min. Tissue was homogenized using an 18G needle, washed with HBSS + 5% FBS, and the cell suspension was filtered through 70 um cell strainer. After washing, the samples were resuspended in 40% Percoll (Cytiva, # 17-0891-01), overlaid with 70% Percoll and centrifuged 850 x g for 20 min at 4°C. The interface was collected and washed with FACS buffer. Fc-gamma receptors were blocked (anti-CD16/32; Biolegend # 101302), and cells were stained with viability dye (LIVE/DEAD Fixable Lime viability kit; ThermoFisher Scientific, # L34989) and antibodies against CD45 (Biolegend, # 160306), CD45.1 (Biolegend, # 110743) CD3 (Biolegend, # 100227, 100206), TCRβ (Biolegend, #109243), TCRγδ (BD Bioscience, #744117), CD4 (Biolegend, # 116027, 300554), CD8a (Biolegend #, 100710, 100706,

155013), TCRvβ 8.1/8.2 (Invitrogen, #11-5813-82), TCRvβ 5.1 (Biolegend, # 139505) Foxp3 Transcription Factor Fixation/Permeabilization kit (eBioscience, # 00-5521-00) was used according to manufacturer's instructions for intracellular staining of perforin (Biolegend # 154306). To assess the total cell counts, Precision Count Beads (Biolegend # 424902) were used. Cells were processed on an Aurora Cytek and analyzed by FlowJo v10 software.

Antibody and tamoxifen treatments. For depletion of T cells, mice were injected via intraperitoneal route with 200 μg of anti-CD4 (InVivoMAb, clone GK1.5, BioXCell # BE0003-1) and/or anti-CD8β (InVivoMAb, Lyt 3.2, clone 53-5.8, BioXCell, # BE0223) or rat isotype control mAb (BioXCell InVivoMAb rat IgG1 anti-horseradish peroxidase, # BE0088; rat IgG2b isotype control, LTF-2, # BE0090) as indicated in the schematics of supplemental Figures. To deplete resident macrophages, mice were injected via intraperitoneal route with 50 mg/kg (1.25 mg) of anti-CSF1R mAb (InVivoMAb, AFS98, BioXCell, # BE0213) or isotype control (rat IgG2a, BioXCell, # BE0089) one day prior to WNV infection and 3 dpi. To decrease monocyte infiltration, mice were injected via intraperitoneal route with 50 μg of anti-CCR2 mAb (clone MC21; (8)) or rat IgG2b isotype control (LTF-2, BioXCell, # BE0090). For combined neutrophil and monocyte depletions, animals were given 250 μg of anti-Ly6G/Ly6C mAb (GR-1, clone NIMP-R14, InVivoMAb, BioXCell, # BE0320) or rat IgG2b isotype control mAb (LTF-2, BioXCell, # BE0090) one day prior to WNV infection and then 2, 4, and 6 dpi. To block IFNγ and TNF, mice were injected via intraperitoneal route with 200 μg of anti-TNF (MP6-XT22, GoInVivo, BioLegend, # 506352) or rat IgG2b isotype control mAb (LTF-2, BioXCell, # BE0090) or anti-IFNγ (Leinco Technologies, # I-438) or Armenian hamster IgG isotype control (Leinco Technologies, # 1196) one day prior to infection and at 2 and 5 dpi.

Tamoxifen (Sigma, # T5648) was resuspended in corn oil and 250 μl of a 20 mg/mL solution was administered via oral gavage to *Ccr2* CreER YFP mice 1 day prior to WNV infection and then at 3, 7 and 11 dpi.

Supplemental Figures

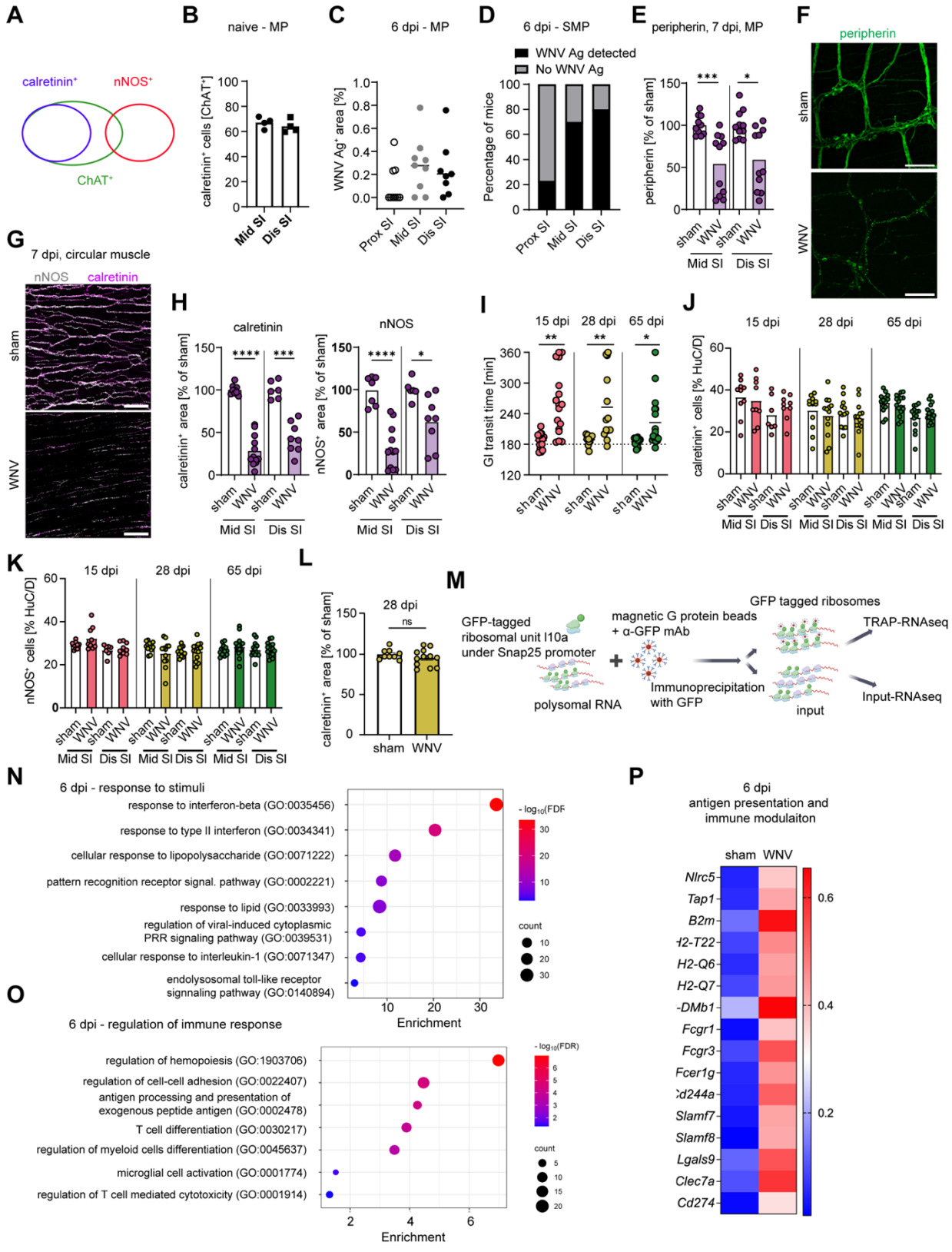

Supplemental Figure S1. WNV tropism and effects on neurons. Related to Figure 1. (**A**) Co-expression of neuronal markers in the myenteric plexus. The diagram shows that most ChAT$^+$ cells also express calretinin and some nNOS. (**B**) Whole mounts of middle and distal SI from sham-infected *ChAT*$^+$ GFP mice after staining for calretinin. Most neurons (70%) co-express both calretinin and ChAT, the residual 30% of neurons express only ChAT; these cells account for the higher percentage of WNV infected cells shown in Figure 1C. (**C, D**) Whole mount preparations of muscularis externa from proximal, mid, and distal SI were isolated at 6 dpi and stained for WNV antigen. (**C**) Data are presented as percentage of WNV antigen positive area in the MP at 6 dpi. (**D**) Muscularis externa was isolated with layer containing submucosal plexus (SMP) at 6 dpi. Data are presented as the percentage of mice with WNV antigen in the SMP. (**E-H, J-L**) Whole mount preparations of muscularis externa from (**E-H**) middle and distal SI or (**L**) proximal SI were isolated at (**E-H**) 7 dpi or (**L**) 28 dpi and stained for (**E, F**) peripherin, (**G, H**) calretinin and nNOS, or (**L**) calretinin. The fraction of area staining positive for neuronal markers in the (**E**) MP or (**H**) circular muscle was determined, and the values were normalized to sham-infected mice. Representative images show staining in mid SI in sham and WNV-infected mice at 7 dpi. Scale bar; 100 μm. (**I**) GI transit time in sham or WNV-infected mice at indicated time points. (**J-K**) Muscularis externa was isolated from the mid and distal regions of SI of sham or WNV-infected mice at 15, 28 or 65 dpi and stained for neuronal markers HuC/D, nNOS, and calretinin. Data are shown as percentage of HuC/D$^+$ neurons. (**M**) Scheme of Translating Ribosome Affinity Purification (TRAP) used for enrichment of RNA from enteric neurons in muscularis externa. (**N-P**) RNAseq analysis of neuron-enriched samples from sham or WNV-infected *Snap25l10a* GFP mice 6 dpi. (**N, O**) Bubble plots of GO pathways represented by differentially expressed genes in sham and WNV-infected mice involved in (**N**) response to stimuli or (**O**) regulation of immune response. (**P**) Heatmap of differentially expressed genes involved in antigen presentation and immune modulation. Gene expression is normalized across each gene and represent the average of 4 samples per condition. Data are pooled from the following number of experiments (left to right): (**B**) 2; (**C**) 2; (**D**) 3; (**E**) 3; (**H**) 3; (**I**) 3, 2, 3; (**J, K**) 2, 3, 4; (**L**) 2; (**N-P**) 1. The indicated numbers of mice per group are shown from left to right: (**B**) 4, 4; (**C**) 9, 9, 9; (**D**) 10, 11, 11, 11; (**E**) 9, 12, 6, 8, 7, 12, 6, 8; (**I**) 17, 12, 13, 13, 1—7; (**J, K**) 10, 9, 7, 9, 13, 13, 13, 13, 14, 16, 14, 16; (**L**) 9, 12; (**N, P**) 4. Lines and column heights indicate mean values. Statistical analysis: (**E, H, I, J, K**) two-tailed Mann-Whitney test: not significant, ns, *$p < 0.05$, **$p < 0.01$.

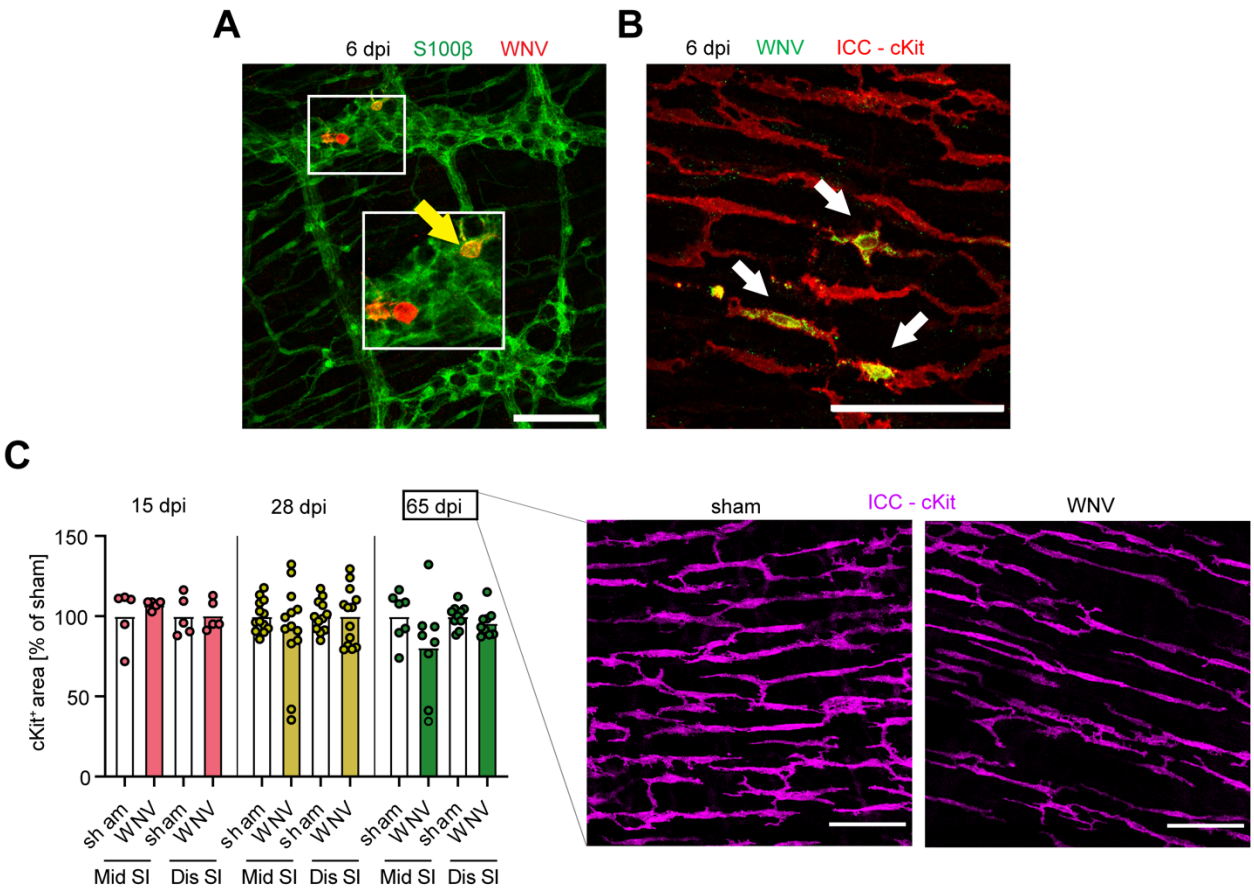

Supplemental Figure S2. Effect of WNV infection on ICCs, Related to Figure 2. (**A-C**) Muscularis externa was isolated from the middle or distal regions of small intestine of sham or WNV-infected wt mice at (**A, B**) 6 dpi or (**C**) 15, 28, or 65 dpi and stained for (**A**) glial marker S100β and WNV antigen or (**B**) ICC marker cKit and WNV antigen. Scale bar, 100 μm. (**C**) The fraction of area staining positive for cKit in the circular muscle layer was determined, and the values were normalized to sham-infected mice. Representative images are from at least 2 experiments. (**B**) White arrows indicate WNV-infected ICCs. Column heights indicate mean values. Data are from (**D**) from left to right: 1, 3, 3 experiments, n = 5, 5, 5, 5, 13, 13, 13, 12, 13, 7, 8, 10, 9 mice.

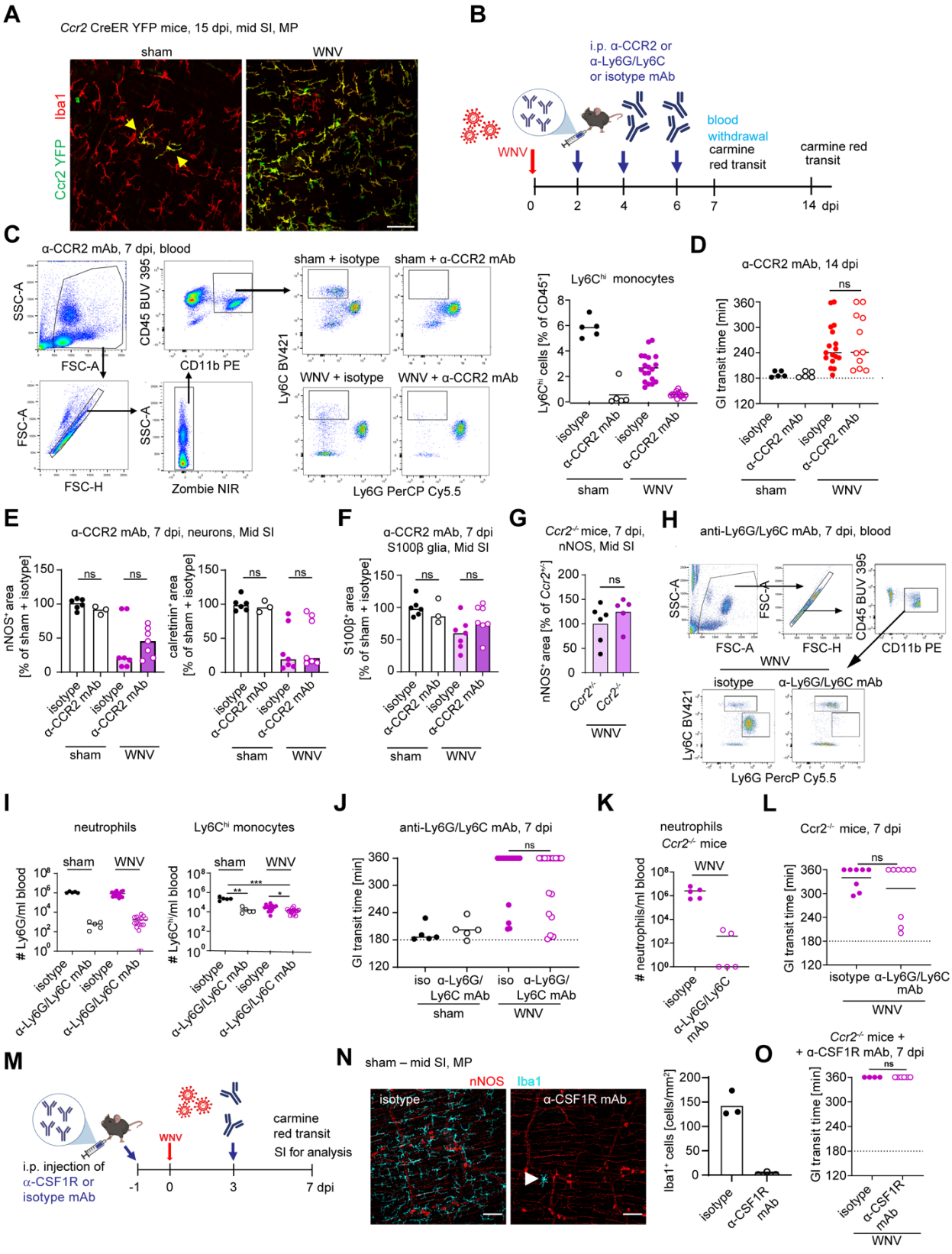
A
Ccr2 CreER YFP mice, 15 dpi, mid SI, MP
sham
WNV
Iba1
Ccr2 YFP
B
i.p. α-CCR2 or
α-Ly6G/Ly6C
or isotype mAb
WNV
blood
withdrawal
carmine
red transit
carmine red
transit
0
2
4
6
7
14 dpi
C
α-CCR2 mAb, 7 dpi, blood
SSC-A
CD45 BUV 395
FSC-A
CD11b PE
FSC-A
SSC-A
FSC-H
Zombie NIR
sham + isotype
sham + α-CCR2 mAb
WNV + isotype
WNV + α-CCR2 mAb
Ly6C BV421
Ly6G PerCP Cy5.5
Ly6C^hi monocytes
Ly6C^hi cells [% of CD45^+]
isotype
α-CCR2 mAb
isotype
α-CCR2 mAb
sham
WNV
D
α-CCR2 mAb, 14 dpi
ns
GI transit time [min]
isotype
α-CCR2 mAb
isotype
α-CCR2 mAb
sham
WNV
E
α-CCR2 mAb, 7 dpi, neurons, Mid SI
nNOS^+ area
[% of sham + isotype]
calretinin^+ area
[% of sham + isotype]
ns
isotype
α-CCR2 mAb
isotype
α-CCR2 mAb
sham
WNV
F
α-CCR2 mAb, 7 dpi
S100β glia, Mid SI
S100β^+ area
[% of sham + isotype]
ns
isotype
α-CCR2 mAb
isotype
α-CCR2 mAb
sham
WNV
G
Ccr2^-/- mice, 7 dpi,
nNOS, Mid SI
nNOS^+ area [% of Ccr2^+/-]
ns
Ccr2^+/-
Ccr2^-/-
WNV
H
anti-Ly6G/Ly6C mAb, 7 dpi, blood
SSC-A
FSC-A
FSC-A
FSC-H
CD45 BUV 395
CD11b PE
WNV
isotype
α-Ly6G/Ly6C mAb
Ly6C BV421
Ly6G PercP Cy5.5
I
neutrophils
Ly6C^hi monocytes
sham
WNV
Ly6G/ml blood
Ly6C^hi/ml blood
isotype
α-Ly6G/Ly6C mAb
isotype
α-Ly6G/Ly6C mAb
J
anti-Ly6G/Ly6C mAb, 7 dpi
ns
GI transit time [min]
iso
α-Ly6G/
Ly6C mAb
iso
α-Ly6G/
Ly6C mAb
sham
WNV
K
neutrophils
Ccr2^-/- mice
WNV
neutrophils/ml blood
isotype
α-Ly6G/Ly6C
mAb
L
Ccr2^-/- mice, 7 dpi
ns
GI transit time [min]
isotype
α-Ly6G/Ly6C
mAb
WNV
M
i.p. injection of
α-CSF1R or
isotype mAb
WNV
carmine
red transit
SI for analysis
-1
0
3
7 dpi
N
sham – mid SI, MP
nNOS
Iba1
isotype
α-CSF1R mAb
O
Iba1^+ cells [cells/mm^2]
isotype
α-CSF1R
mAb
Ccr2^-/- mice +
+ α-CSF1R mAb, 7 dpi
ns
GI transit time [min]
isotype
α-CSF1R
mAb
WNV

Supplemental Figure S3. Infiltrating monocytes and macrophages do not contribute to WNV-induced damage to neurons and glia and ensuing GI dysmotility, Related to Figure 3. (**A, E, F, G, N**) Muscularis externa was isolated from the (**A, G, N**) middle or (**E, F**) middle and distal region of small intestine (SI) of (**A**) sham or WNV-infected *Ccr2* CreER YFP mice at 15 dpi, (**E, F**) sham or WNV-infected wt mice treated with anti-CCR2 Ab at 7 dpi, (**G**) WNV-infected $Ccr2^{-/+}$ and $Ccr2^{-/-}$ mice at 7 dpi, or (**N**) sham mice treated with anti-CSF1R mAb and stained for (**A**) macrophage marker Iba1, (**E, F**) calretinin and nNOS, (**G**) nNOS, or (**N**) Iba1 and nNOS. (**A**) Representative images are from the middle region of SI of 3 mice per group. Scale bar, 100 μm. (**E, F, G**) The fraction of positive area for (**E**) calretinin and nNOS, (**F**) S100β, (**G**) nNOS in the MP was determined, and values were normalized to (**E, F**) sham-infected wt mice treated with isotype mAb or (**G**) to WNV-infected *Ccr2*$^{+/-}$ mice. (**N**) $Iba1^+$ cells were counted in the MP, and cell counts are expressed as the number of $Iba1^+$ cells per mm^2. (**B**) Experimental design of monocyte/neutrophil depletion after WNV infection using anti-CCR2 or Ly6G/Ly6C mAb treatments. GI transit was assessed at 7 dpi (anti-CCR2 and anti-Ly6G/Ly6C and treated groups) or 14 dpi (only CCR2 mAb-treated group). Blood was obtained at 7 dpi. (**C, H, I, K**) Leukocytes from sham or WNV-infected (**C, H, I**) wt or (**K**) *Ccr2*$^{-/-}$ mice treated with (**C**) anti-CCR2 mAb or (**H, I, K**) anti-Ly6G/Ly6C mAb were stained with antibodies to CD45, CD11b, Ly6G, and Ly6C. (**C**) Percentages and (**I, K**) numbers (**C**) of monocytes ($CD45^+$ $CD11b^+$ $Ly6G^-$ $Ly6C^{hi}$) and/or (**I, K**) neutrophils ($CD45^+$ $CD11b^+$ $Ly6G^+$ $Ly6C^+$). (**C, H**). Gating strategy of (**C**) monocyte and (**H**) monocyte/neutrophil populations by flow cytometry. (**D, J, L, O**) GI transit was measured in (**D**) in sham or WNV-infected mice after treatment with anti-CCR2 or isotype mAbs at 14 dpi, (**J**) in sham or WNV-infected mice after treatment with anti-Ly6G/Ly6C, or isotype control mAb at 7 dpi, (**L**) WNV-infected *Ccr2*$^{-/-}$ mice treated with anti-Ly6G/Ly6C or isotype control mAb at 7 dpi or (**O**) WNV infected *Ccr2*$^{-/-}$ mice treated with anti-CSF1R or isotype mAb at 7 dpi. Data are pooled from the following number of experiments: (**C, D, H, G**) 3; (**E, F, L, N, O**) 2; and (**I**) 1. The indicated numbers of mice per group are shown from left to right: (**C**) 5, 5, 20,15; (**D**) 5, 5, 17, 11; (**E, F**) 6, 3, 7, 7; (**G**) 6, 5; (**I, J**) 5, 5, 20, 15; (**K**) 5, 5; (**L**) 8, 9; (**N**) 3, 3 and (**O**) 4, 6. Lines and column heights indicate mean values. Statistical analysis: (**D, E, F, G, K, L, O**) two-tailed Mann-Whitney test; (**I**) Kruskal-Wallis ANOVA with Dunn's post-test. Not significant, ns, *$p < 0.05$, **$p < 0.01$, ***$p < 0.001$.

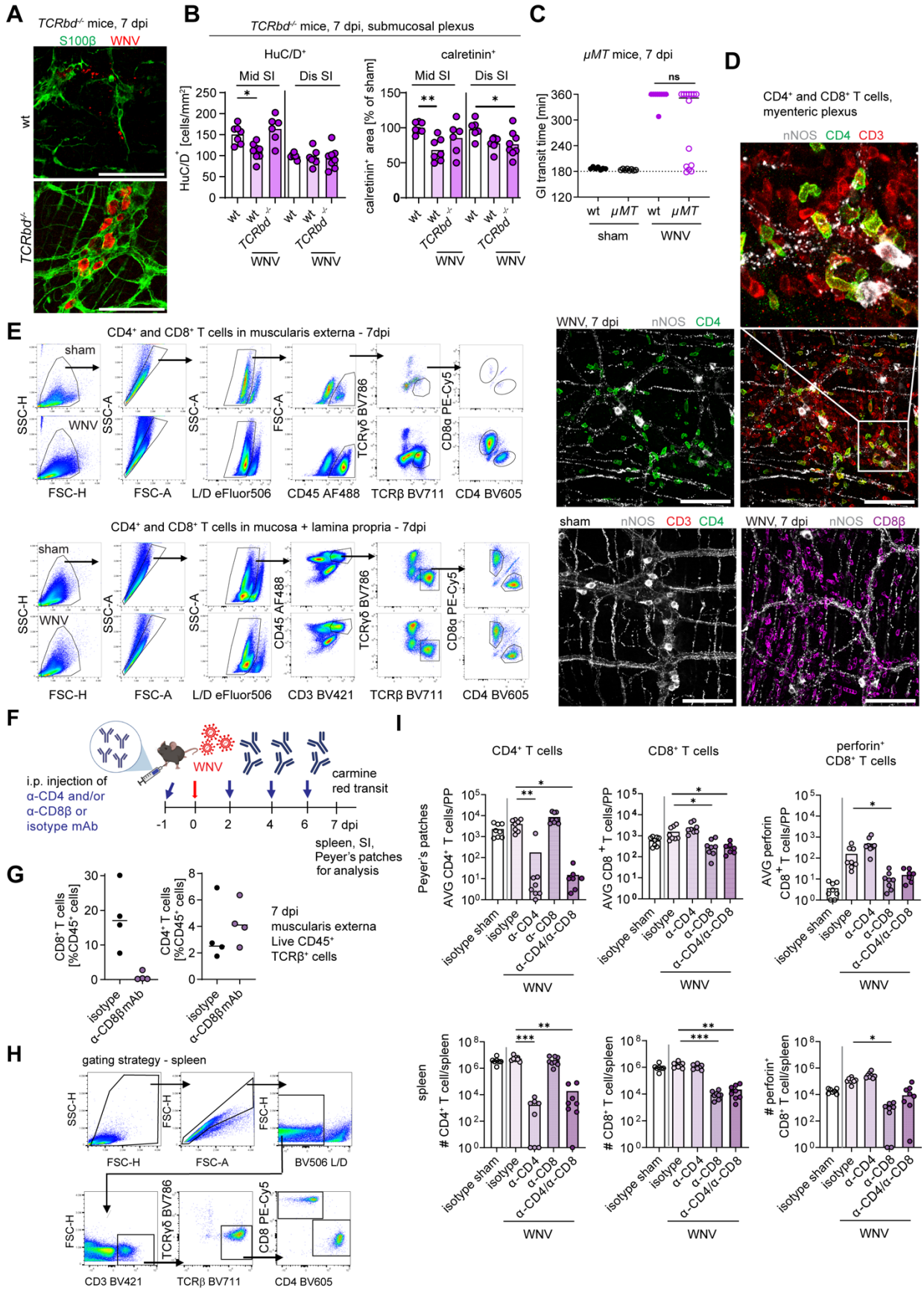
A
TCRbd-/- mice, 7 dpi
S100β WNV
wt
TCRbd-/-
B
TCRbd-/- mice, 7 dpi, submucosal plexus
HuC/D+
Mid SI Dis SI
HuC/D+ [cells/mm²]
calretinin+
calretinin+ area [% of sham]
wt wt -/- TCRbd -/-
WNV
C
μMT mice, 7 dpi
ns
GI transit time [min]
wt μMT wt μMT
sham WNV
D
CD4+ and CD8+ T cells, myenteric plexus
nNOS CD4 CD3
WNV, 7 dpi nNOS CD4
sham nNOS CD3 CD4
WNV, 7 dpi nNOS CD8β
E
CD4+ and CD8+ T cells in muscularis externa - 7dpi
sham
WNV
SSC-H
FSC-H
SSC-A
FSC-A
L/D eFluor506
CD45 AF488
FSC-A
TCRγδ BV786
CD8α PE-Cy5
TCRβ BV711
CD4 BV605
CD4+ and CD8+ T cells in mucosa + lamina propria - 7dpi
CD3 BV421
F
WNV
i.p. injection of
α-CD4 and/or
α-CD8β or
isotype mAb
carmine red transit
-1 0 2 4 6 7 dpi
spleen, SI, Peyer's patches for analysis
G
CD8+ T cells [%CD45+ cells]
CD4+ T cells [%CD45+ cells]
isotype α-CD8βmAb
7 dpi
muscularis externa
Live CD45+
TCRβ+ cells
H
gating strategy - spleen
FSC-H
FSC-A
BV506 L/D
CD3 BV421
TCRβ BV711
CD4 BV605
I
CD4+ T cells
CD8+ T cells
perforin+ CD8+ T cells
Peyer's patches
AVG CD4+ T cells/PP
AVG CD8+ T cells/PP
AVG perforin CD8+ T cells/PP
spleen
CD4+ T cell/spleen
CD8+ T cell/spleen
perforin+ CD8+ T cell/spleen
isotype sham isotype α-CD4 α-CD8 α-CD4/α-CD8
WNV

Supplemental Figure S4. $CD4^+$ and $CD8^+$ T cells contribute to WNV-triggered ENS injury and GI dysmotility, Related to Figure 4. (**A, B, D**) Whole mount preparations of muscularis externa were isolated from WNV-infected wt and *TCRbd*$^{-/-}$ mice at 7 dpi and co-stained for (**A**) WNV antigen and glia (S100β), (**B**) HuC/D and calretinin or (**D**) T cell markers CD3, CD4 or CD8, and nNOS. Representative images from (**A**) 2 experiments or (**D**) of at least 3 mice, scale bar, 100 μm. (**B**) The fraction of positive area for calretinin in the SMP was determined, and values were normalized to sham-infected wt mice. HuC/D^+ cells were counted in the SMP, and cell counts are expressed as the number of HuC/D^+ cells per mm^2. Values for wt mice are shown for comparison and are identical to those shown in Figure 1E. (**C**) GI transit time of sham or WNV-infected wt or *μMT* mice at 7 dpi. (**E, G**) Flow cytometric analysis of small intestine at 7 dpi. (**E**) Gating strategy and (**G**) proportions of $CD4^+$ and $CD8^+$ T cell populations in (**E**) muscularis externa or mucosa and lamina propria (residual) or (**G**) muscularis externa of wt mice treated with anti-CD8β mAb. (**F**) Experimental design of T cell depletions. Mice were injected with anti-CD4, anti-CD8β, or both anti-CD4 and CD8 mAbs. (**H, I**) $CD4^+$ and $CD8^+$ T cells (**G**) in muscularis externa or (**I**) in spleen and Peyer's patches harvested from sham or WNV-infected mice treated with anti-CD4/CD8 or isotype mAb and stained for CD45, CD3, TCRβ, TCRγδ, CD4, CD8α, and perforin and gated on (**G**) live $CD45^+$ $TCR\beta^+$ $TCR\gamma\delta^-$ or (**I**) live $CD3^+$ $TCR\beta^+$ $TCR\gamma\delta^-$ $CD4^+$ or $CD8^+$ T cells (shown in **H**). Data are shown as (**G**) percentage of $CD45^+$ cells in SI and (**I**) total cell numbers per spleen and average cell numbers per Peyer's patch. Data are pooled from the following number of experiments: (**B**) 3, (**C**) 3, (**G**) 1, (**I**) 2. The indicated numbers of mice are shown per group (left to right): (**B**) 7, 8, 6, 6, 7, 8, 7, 7, 6, 6, 7, 8; (**C**) 7, 8, 9, 14; (**G**) 4, 4, 4, 4; (**I**); 8, 8, 8, 8, 7 (Peyer's patches), 7, 8, 8, 8, 8 (spleen). Lines indicate median values. Column heights indicate mean values. Statistical analysis: (**C**) two-tailed Mann-Whitney test; (**B, H**) Kruskal-Wallis ANOVA with Dunn's post-test comparisons were to "wt sham" (**B**) or "isotype WNV control" (**H**) groups: not significant, ns, *$p < 0.05$, **$p < 0.01$, ***$p < 0.001$.

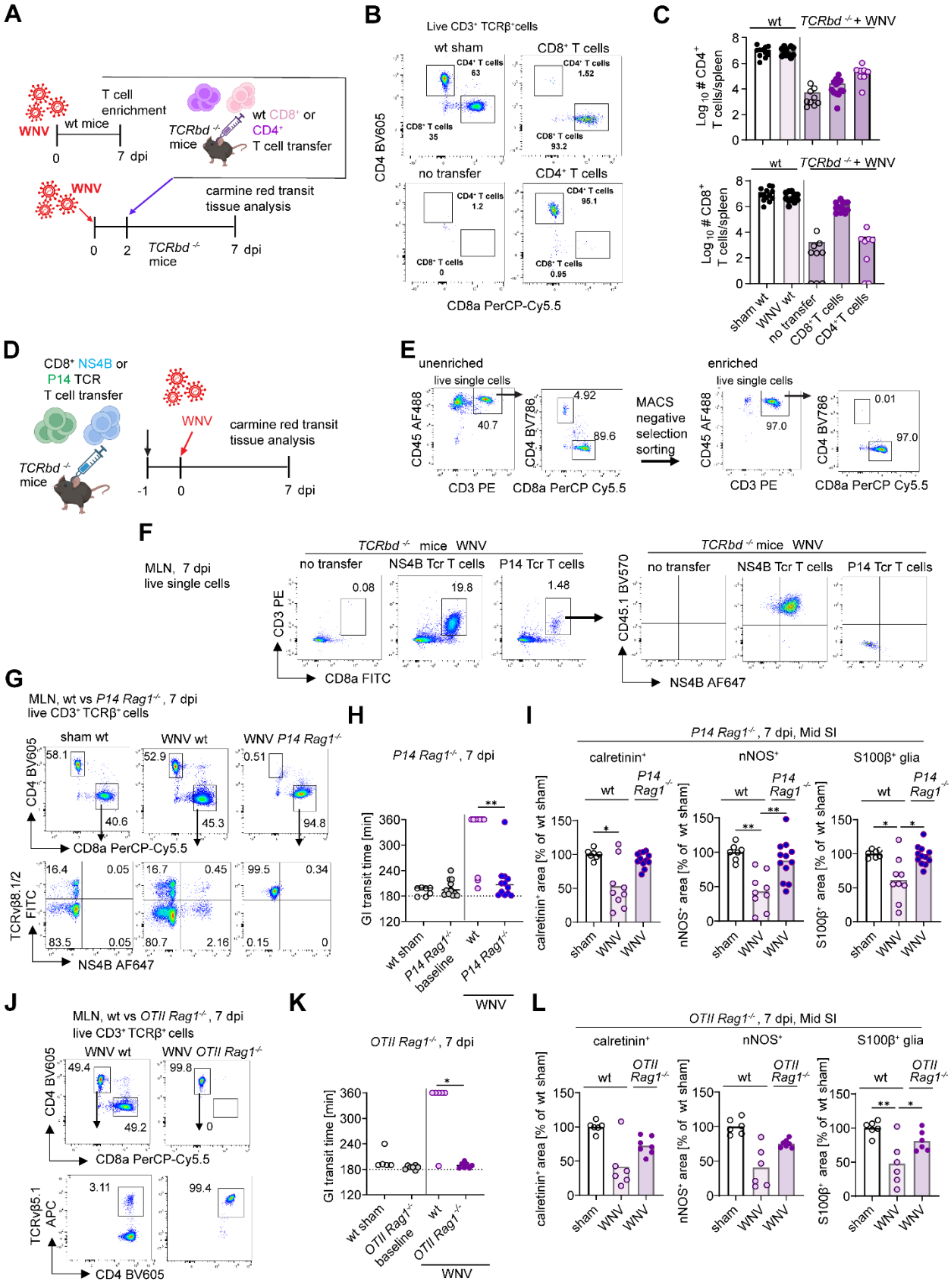
A
WNV
wt mice
T cell enrichment
0
7 dpi
TCRbd -/- mice
wt CD8+ or CD4+ T cell transfer
WNV
carmine red transit tissue analysis
0 2 TCRbd -/- mice 7 dpi
B
Live CD3+ TCRβ+cells
wt sham
CD8+ T cells
no transfer
CD4+ T cells
CD4 BV605
CD8a PerCP-Cy5.5
C
wt TCRbd -/- + WNV
Log10 # CD4+ T cells/spleen
Log10 # CD8+ T cells/spleen
sham wt
WNV wt
no transfer
CD8+T cells
CD4+T cells
D
CD8+ NS4B or P14 TCR T cell transfer
TCRbd -/- mice
WNV
carmine red transit tissue analysis
-1 0 7 dpi
E
unenriched
live single cells
CD45 AF488
CD3 PE
CD4 BV786
CD8a PerCP Cy5.5
MACS negative selection sorting
enriched
F
MLN, 7 dpi
live single cells
TCRbd -/- mice WNV
no transfer
NS4B Tcr T cells
P14 Tcr T cells
CD3 PE
CD8a FITC
CD45.1 BV570
NS4B AF647
G
MLN, wt vs P14 Rag1-/-, 7 dpi
live CD3+ TCRβ+ cells
sham wt
WNV wt
WNV P14 Rag1-/-
CD4 BV605
CD8a PerCP-Cy5.5
TCRvβ8.1/2 FITC
NS4B AF647
H
P14 Rag1-/-, 7 dpi
GI transit time [min]
wt sham
P14 Rag1-/- baseline
wt
P14 Rag1-/-
WNV
I
P14 Rag1-/-, 7 dpi, Mid SI
calretinin+
nNOS+
S100β+ glia
wt
P14 Rag1-/-
calretinin+ area [% of wt sham]
nNOS+ area [% of wt sham]
S100β+ area [% of wt sham]
sham
WNV
J
MLN, wt vs OTII Rag1-/-, 7 dpi
live CD3+ TCRβ+ cells
WNV wt
WNV OTII Rag1-/-
CD4 BV605
CD8a PerCP-Cy5.5
TCRvβ5.1 APC
K
OTII Rag1-/-, 7 dpi
GI transit time [min]
wt sham
OTII Rag1-/- baseline
wt
OTII Rag1-/-
WNV
L
OTII Rag1-/-, 7 dpi, Mid SI
calretinin+
nNOS+
S100β+ glia
wt
OTII Rag1-/-
calretinin+ area [% of wt sham]
nNOS+ area [% of wt sham]
S100β+ area [% of wt sham]
sham
WNV

Supplemental Figure S5. Damage to neuronal and glial network is caused by WNV-specific CD4$^+$ and CD8$^+$ T cells, Related to Figure 5. (**A**) Experimental design of adoptive transfer of wt CD8$^+$ or CD4$^+$ T cells to *TCRbd*$^{-/-}$ mice. CD8$^+$ (5 x 10^6) or CD4$^+$ (10^7) T cells from wt spleens and MLNs at 7 dpi were enriched and injected intravenously into WNV-infected *TCRbd*$^{-/-}$ mice at 2 dpi. (**B, C**) Flow cytometric analysis of splenocytes from *TCRbd*$^{-/-}$ mice after transfer of primed wt T cells at 7 dpi. Spleens were harvested and stained for CD3, TCRβ, TCRγδ, CD4 and CD8α and gated on live CD3$^+$ TCRβ$^+$ TCRγδ$^-$ CD4$^+$ or CD8$^+$ T cells. (**B**) Representative flow cytometry dot plots and (**C**) total cell numbers per spleen. (**D**) *TCRbd*$^{-/-}$ mice were adoptively transferred by intravenous injection with 10^6 WNV NS4B or LCMV P14 gp33 transgenic CD8$^+$ T cells and then inoculated subcutaneously with WNV one day later. (**E, F**) Representative flow cytometry dot plots of (**E**) splenocytes before and after enrichment for NS4B and LCMV P14 gp33 transgenic CD8$^+$ T cells and (**F**) of T cells from mesenteric lymph nodes of *TCRbd*$^{-/-}$ mice injected with NS4B or P14 transgenic T cells at 7 dpi. Cells were stained with mAbs against (**E**) CD45, CD3, CD4 and CD8α and gated on live CD45$^+$ CD3$^+$ CD4$^+$ or CD8$^+$ T cells or (**F**) CD45.1 (to identify NS4B transgenic CD8$^+$ T cells), CD3, CD8a, and WNV NS4B D^b-restricted tetramers and gated on live cells. (**G, J**) Flow cytometric analysis of cells in MLNs from WNV-infected wt or (**G**) wt sham or WNV-infected *P14 Rag1*$^{-/-}$ mice or (**J**) WNV-infected *OT-II Rag1*$^{-/-}$ mice at 7 dpi. MLNs were harvested at 7 dpi and stained for CD3, TCRβ, TCRγδ, CD4, CD8α and (**G**) TCRvβ 8.1/8.2 specific for LCMV and WNV NS4B D^b-restricted tetramers or (**J**) TCR vβ 5.1 specific for OVA and gated on live CD3$^+$ TCRβ$^+$ TCRγδ$^-$ CD4$^+$ or CD8$^+$ T cells. (**H, K***)* GI transit was measured at 7 dpi. Transit time of (**H**) sham-infected or WNV-infected wt or *P14 Rag1*$^{-/-}$ mice or (**K**) WNV-infected *OT-II Rag1*$^{-/-}$ mice. (**I, L**) Muscularis externa was isolated from the mid regions of small intestine (SI) of (**I**) sham-infected or WNV-infected wt or *P14 Rag1*$^{-/-}$ mice or (**L**) WNV-infected *OT-II Rag1*$^{-/-}$ mice at 7 dpi and stained. The fraction of area positive for calretinin, nNOS or S100β was determined, and values were normalized to wt sham mice. Data are pooled from (**C, G, H, I**) 3 and (**J, K, L**) 2 experiments with indicated numbers of mice per group (left to right): (**C**) 4, 5, 4, 4, 4; (**H**) 7, 10, 12, 12; (**I**) 7, 9, 12, 7, 9, 12, 7, 9, 12; (**K**) 5, 6, 9, 9; (**L**) 6, 6, 7, 7. Representative flow plots are from (**E, F, G**) 3 or (**J**) 2 experiments. Lines and column heights indicate the mean values. Statistical analysis: (**H, K**) two-tailed Mann-Whitney test; (**I, L**) Kruskal-Wallis one-way ANOVA with Dunn's post-test: not significant, ns, *$p < 0.05$, **$p < 0.01$, ***$p < 0.001$.

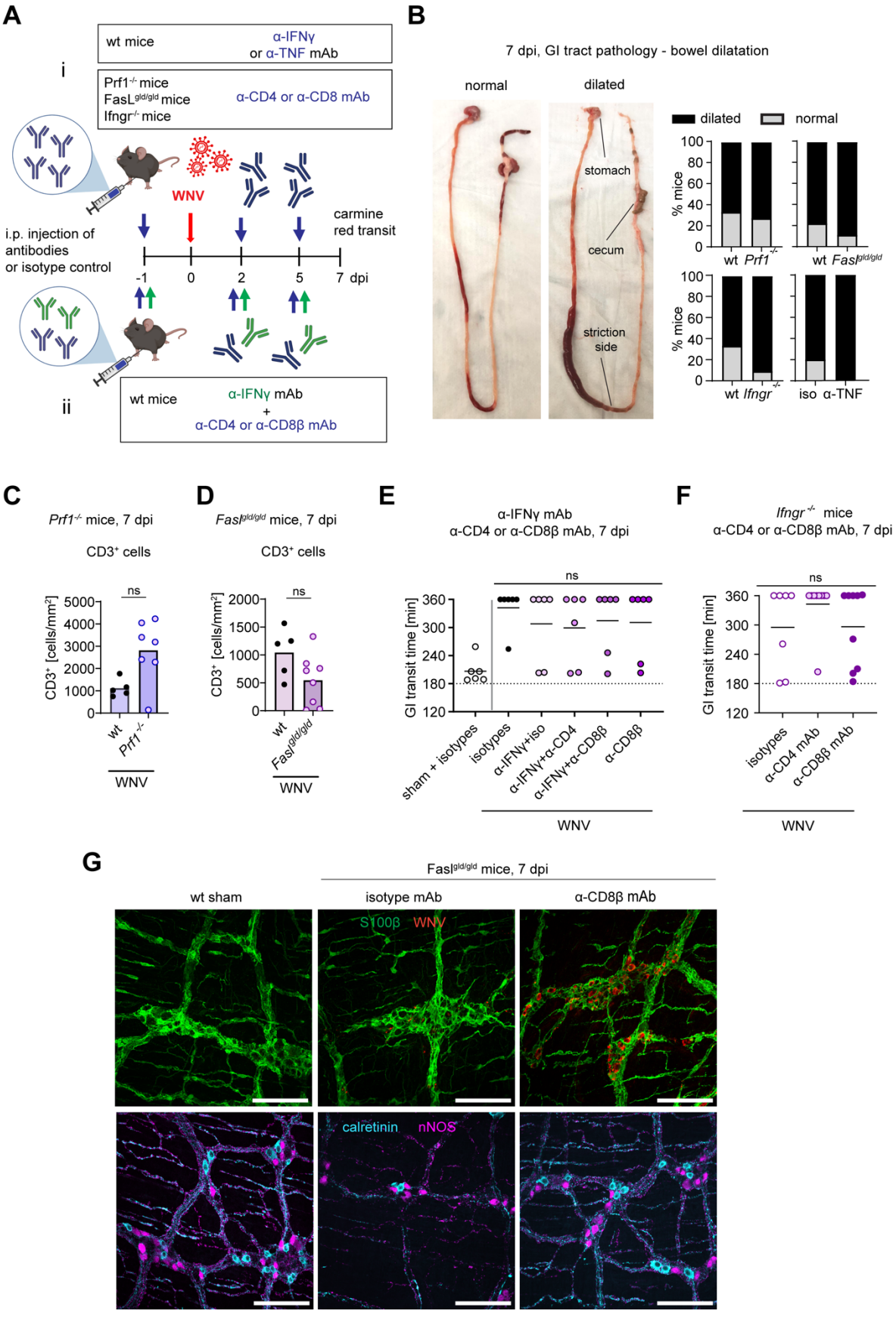
A
wt mice
α-IFNγ
or α-TNF mAb
i
Prf1-/- mice
FasLgld/gld mice
Ifngr-/- mice
α-CD4 or α-CD8 mAb
WNV
carmine
red transit
i.p. injection of
antibodies
or isotype control
-1
0
2
5
7 dpi
ii
wt mice
α-IFNγ mAb
+
α-CD4 or α-CD8β mAb
B
7 dpi, GI tract pathology - bowel dilatation
normal
dilated
stomach
cecum
striction
side
dilated
normal
% mice
wt Prf1-/-
wt Faslgld/gld
wt Ifngr-/-
iso α-TNF
C
Prf1-/- mice, 7 dpi
CD3+ cells
CD3+ [cells/mm2]
ns
wt
Prf1-/-
WNV
D
Faslgld/gld mice, 7 dpi
CD3+ cells
CD3+ [cells/mm2]
ns
wt
Faslgld/gld
WNV
E
α-IFNγ mAb
α-CD4 or α-CD8β mAb, 7 dpi
GI transit time [min]
ns
sham + isotypes
isotypes
α-IFNγ+iso
α-IFNγ+α-CD4
α-IFNγ+α-CD8β
α-CD8β
WNV
F
Ifngr-/- mice
α-CD4 or α-CD8β mAb, 7 dpi
GI transit time [min]
ns
isotypes
α-CD4 mAb
α-CD8β mAb
WNV
G
Faslgld/gld mice, 7 dpi
wt sham
isotype mAb
α-CD8β mAb
S100β
WNV
calretinin
nNOS

Supplemental Figure S6. Damage to neuronal and glial network is caused by multiple effector functions of T cells, Related to Figures 6 and 7. (**A**) Experimental design of (**i**) T cell depletion in *Prf1*$^{-/-}$, *Fasl*$^{gld/gld}$, *Ifngr*$^{-/-}$ mice or IFNγ or TNF blockade in wt mice and (**ii**) combined T cell depletion and IFNγ blockade in wt mice after WNV infection using anti-CD4, anti-CD8β, and anti-IFNγ mAb treatments as indicated. GI transit was assessed at 7 dpi. (**B**) Proportions of wt or *Prf1*$^{-/-}$, *Fasl*$^{gld/gld}$, *Ifngr*$^{-/-}$ or wt mice treated with anti-TNF blocking mAb or isotype control mAb with abnormally dilated bowel at 7 dpi. (**C, D**) Whole mount preparations of muscularis externa were isolated from WNV-infected wt and (**C**) *Prf1*$^{-/-}$ or (**D**) *Fasl*$^{gld/gld}$ mice at 7 dpi and stained for T cell marker CD3. Numbers of $CD3^+$ cells in the myenteric plexus were calculated by dividing the area positive for $CD3^+$ staining with average size of $CD3^+$ cell. Cell counts are expressed as numbers of $CD3^+$ cells per mm^2. (**E, F**) GI tract transit was measured at 7 dpi in wt mice treated with (**E**) anti-IFNγ in combination with anti-CD4 or anti-CD8β mAb or isotype control mAb or (**F**) in *Ifngr*$^{-/-}$ mice treated with anti-CD4 or anti-CD8β mAb or isotype control mAb. (**G**) Representative staining images of the myenteric plexus are from middle region of small intestine (SI) in wt sham, WNV-infected *Fasl*$^{gld/gld}$ mice treated with anti-CD8β or isotype mAb at 7 dpi. Scale bar, 100 μm. Data are pooled from (**B**) 2 , (**C, D**) 2,(**E**) 2, (**F**) 3 experiments with indicated numbers of mice per group (left to right): (**B**) 5, 11, 9, 9, 10, 10; (**C**) 5, 7; (**D**) 5, 8 ;(**E**) 6, 6, 6, 6, 6, 6 (**F**) 7, 9, 9. (**G**) Representative images of 3 experiments. . Lines and column heights indicate the mean values. Statistical analysis: (C, D) two-tailed Mann-Whitney test; (**E, F**) ANOVA with Dunnett's post-test (comparison to "WNV isotype control" group): not significant, ns.

Supplemental References

1. Diamond MS, Shrestha B, Marri A, Mahan D, and Engle M. B cells and antibody play critical roles in the immediate defense of disseminated infection by West Nile encephalitis virus. *J Virol.* 2003;77(4):2578-86.
2. Dobin A, Davis CA, Schlesinger F, Drenkow J, Zaleski C, Jha S, et al. STAR: ultrafast universal RNA-seq aligner. *Bioinformatics.* 2013;29(1):15-21.
3. Liao Y, Smyth GK, and Shi W. featureCounts: an efficient general purpose program for assigning sequence reads to genomic features. *Bioinformatics.* 2014;30(7):923-30.
4. Patro R, Duggal G, Love MI, Irizarry RA, and Kingsford C. Salmon provides fast and bias-aware quantification of transcript expression. *Nat Methods.* 2017;14(4):417-9.
5. Love MI, Huber W, and Anders S. Moderated estimation of fold change and dispersion for RNA-seq data with DESeq2. *Genome Biol.* 2014;15(12):550.
6. Ashburner M, Ball CA, Blake JA, Botstein D, Butler H, Cherry JM, et al. Gene ontology: tool for the unification of biology. The Gene Ontology Consortium. *Nat Genet.* 2000;25(1):25-9.
7. Aleksander SA, Balhoff J, Carbon S, Cherry JM, Drabkin HJ, Ebert D, et al. The Gene Ontology knowledgebase in 2023. *Genetics.* 2023;224(1).
8. Mack M, Cihak J, Simonis C, Luckow B, Proudfoot AE, Plachý J, et al. Expression and characterization of the chemokine receptors CCR2 and CCR5 in mice. *J Immunol.* 2001;166(7):4697-704.